TKK Dissertations 134
Espoo 2008

AVALANCHE DYNAMICS IN DRIVEN SYSTEMS: FROM PLASTIC DEFORMATION TO FLUID INVASION

Doctoral Dissertation

Lasse Laurson

Helsinki University of Technology
Faculty of Information and Natural Sciences
Department of Engineering Physics

TKK Dissertations 134
Espoo 2008

AVALANCHE DYNAMICS IN DRIVEN SYSTEMS: FROM PLASTIC DEFORMATION TO FLUID INVASION

Doctoral Dissertation

Lasse Laurson

Dissertation for the degree of Doctor of Science in Technology to be presented with due permission of the Faculty of Information and Natural Sciences for public examination and debate in Auditorium N at Helsinki University of Technology (Espoo, Finland) on the 30th of September, 2008, at 13 o'clock.

Helsinki University of Technology
Faculty of Information and Natural Sciences
Department of Engineering Physics

Teknillinen korkeakoulu
Informaatio- ja luonnontieteiden tiedekunta
Teknillisen fysiikan laitos

Distribution:
Helsinki University of Technology
Faculty of Information and Natural Sciences
Department of Engineering Physics
P.O. Box 1100
FI - 02015 TKK
FINLAND
URL: http://tfy.tkk.fi/
Tel. +358-9-451 3231
Fax +358-9-451 3116
E-mail: lasse.laurson@tkk.fi

© 2008 Lasse Laurson

ISBN 978-951-22-9536-4
ISBN 978-951-22-9537-1 (PDF)
ISSN 1795-2239
ISSN 1795-4584 (PDF)
URL: http://lib.tkk.fi/Diss/2008/isbn9789512295371/

TKK-DISS-2500

Picaset Oy
Helsinki 2008

ABSTRACT OF DOCTORAL DISSERTATION	HELSINKI UNIVERSITY OF TECHNOLOGY P. O. BOX 1000, FI-02015 TKK http://www.tkk.fi

Author Lasse Laurson

Name of the dissertation

Avalanche dynamics in driven systems: From plastic deformation to fluid invasion

Manuscript submitted 09.06.2008	Manuscript revised 12.08.2008
Date of the defence 30.09.2008 at 13 o'clock, TKK main building, Otakaari 1, lecture hall N	
☐ Monograph	☒ Article dissertation (summary + original articles)

Faculty	Faculty of Information and Natural Sciences
Department	Department of Engineering Physics
Field of research	Statistical physics
Opponent(s)	Prof. Michael Zaiser, University of Edinburgh
Supervisor	Acad. Prof. Risto Nieminen
Instructor	Doc. Mikko Alava

Abstract

A large class of interacting systems in Nature respond to externally applied driving in an intermittent and heterogeneous manner. Typically, the statistics of sizes of the observed bursts of activity, or avalanches, can be described by scale free power law distributions. Also the temporal correlations associated to such an activity time series are of interest, and can be studied by computing the power spectrum of the time series. This power spectrum typically scales as a power law of the frequency, $1/f^{\alpha}$, thus constituting an example of $1/f$ noise, a phenomenon ubiquitous in Nature.

In this thesis a number of simplified model systems exhibiting such phenomenology are studied, both analytically and by computer simulations. In particular, a relation between the avalanche and noise descriptions of the intermittent activity, originally proposed in the context of Barkhausen noise, is shown to apply more generally to systems with avalanche dynamics. This has important implications especially in the context of sandpile models of self-organized criticality, as it allows to demonstrate how such models can exhibit non-trivial scaling of the power spectra, contrary to earlier claims. The general nature of this relation is further emphasized by showing that it applies also in the apparently very different context of a propagating fluid front when a fluid invades porous media as a sequence of avalanches, as well as for avalanches of plastic deformation activity in a simple two dimensional discrete dislocation dynamics model.

For the dislocation model, also other issues such as correlations between different avalanches and history dependent response to externally applied stresses are studied. An effort is made to understand the role of grain boundaries to the propagation of dislocation avalanches in plastically deforming polycrystals, by studying the screening effect arising from the deformation of a simplified grain boundary in the stress field of a single edge dislocation. Finally, a simple random walk-based model mimicking a dislocation interacting with a cloud of diffusing solute atoms in metallic alloys is studied. Such a system is shown to exhibit fluctuations characterized by power-law distributions with a cut-off.

Keywords avalanches, noise, self-organized criticality, plastic deformation, imbibition	
ISBN (printed) 978-951-22-9536-4	ISSN (printed) 1795-2239
ISBN (pdf) 978-951-22-9537-1	ISSN (pdf) 1795-4584
Language English	Number of pages 49 p. + app. 48 p.
Publisher Department of Engineering Physics, Helsinki University of Technology	
Print distribution Department of Engineering Physics, Helsinki University of Technology	
☒ The dissertation can be read at http://lib.tkk.fi/Diss/2008/isbn9789512295371/	

VÄITÖSKIRJAN TIIVISTELMÄ	TEKNILLINEN KORKEAKOULU PL 1000, 02015 TKK http://www.tkk.fi

Tekijä Lasse Laurson

Väitöskirjan nimi

Vyörydynamiikka ajetuissa systeemeissä: Plastisesta deformaatiosta nesteiden imeytymiseen

Käsikirjoituksen päivämäärä 09.06.2008	Korjatun käsikirjoituksen päivämäärä 12.08.2008

Väitöstilaisuuden ajankohta 30.09.2008 klo 13, Teknillisen korkeakoulun päärakennus, Otakaari 1, sali N

☐ Monografia	☒ Yhdistelmäväitöskirja (yhteenveto + erillisartikkelit)

Tiedekunta	Informaatio- ja luonnontieteiden tiedekunta
Laitos	Teknillisen fysiikan laitos
Tutkimusala	Tilastollinen fysiikka
Vastaväittäjä(t)	Prof. Michael Zaiser, University of Edinburgh
Työn valvoja	Akat. Prof. Risto Nieminen
Työn ohjaaja	Dos. Mikko Alava

Tiivistelmä

Vuorovaikuttavien systeemien vaste ulkoiseen ajavaan voimaan on tyypillisesti epäsäännöllinen ja heterogeeninen. Tällöin havaittavien aktiviteettipurskeiden, tai -vyöryjen, kokojakaumaa kuvaa usein skaalavapaa potenssilakijakauma. Vaihtoehtoinen tapa karakterisoida tällaista purskeista aktiviteettiaikasarjaa on tutkia sen aikakorrelaatioita laskemalla aikasarjan tehospektri, joka tyypillisesti on potenssilakimuotoa $1/f^{\alpha}$, missä f on taajuus. Kyseessä on siis esimerkki $1/f$-kohinasta, joka on luonnossa hyvin yleinen mutta usein huonosti ymmärretty ilmiö.

Tässä väitöskirjassa tutkitaan useita yksinkertaisia mallisysteemejä joissa esiintyy edellä kuvatun kaltaisia ilmiöitä. Tutkimus koostuu sekä analyyttisistä laskuista että tietokonesimulaatioista. Erityisesti tutkimuksessa osoitetaan että tietty yhteys vyöry- ja kohinakuvauksien välillä, joka on alunperin esitetty Barkhausenin ilmiön yhteydessä, on voimassa varsin yleiseti vyörydynamiikkasysteemeissä. Tällä on merkittäviä seurauksia mm. itseorganisoituvasti kriittisten n.s. hiekkakasamallien osalta, sillä kyseinen relaatio osoittaa näissä malleissa esiintyvän monimutkaisia aikakorrelaatioita, vastoin aikaisempaa käsitystä. Tämä purskeisten signaalien vyöry- ja kohinakuvausten välinen yhteys on luonteeltaan varsin yleinen: Se on voimassa myös näennäisesti hyvin erilaisessa systeemissä, nimittäin nesterajapinnan vyörymäisessä etenemisessä nesteen tunkeutuessa huokoiseen aineeseen kapillaarivoimien vaikutuksesta. Sama relaatio pätee myös plastisen deformaation vyöryille yksinkertaisessa kaksiulotteisessa diskreetissä dislokaatiodynamiikkamallissa.

Dislokaatiomallissa tutkitaan myös muita ilmiöitä, kuten eri vyöryjen välisiä korrelaatioita sekä historiasta riippuvaa vastetta ulkoiseen voimaan. Myös monikiteisissä aineissa esiintyvien raerajojen merkitystä plastisen deformaation vyöryjen etenemiselle tarkastellaan tutkimalla yksinkertaisen raerajamallin yksittäisen dislokaation jännityskentässä tapahtuvasta deformaatiosta seuravaa varjostusefektiä. Lopuksi tutkitaan yksittäisen hiukkasen dynamiikkaa sen vuorovaikuttaessa diffundoituvien epäpuhtausatomien kanssa, ja osoitetaan että systeemissä esiintyviä fluktuaatioita voidaan karakterisoida potenssilakijakaumilla.

Asiasanat	vyöryt, kohina, itseorganisoituva kriittisyys, plastinen muodonmuutos, imbibitio
ISBN (painettu) 978-951-22-9536-4	ISSN (painettu) 1795-2239
ISBN (pdf) 978-951-22-9537-1	ISSN (pdf) 1795-4584
Kieli englanti	Sivumäärä 49 s. + liit. 48 s.
Julkaisija	Teknillisen fysiikan laitos, Teknillinen korkeakoulu
Painetun väitöskirjan jakelu	Teknillisen fysiikan laitos, Teknillinen korkeakoulu

☒ Luettavissa verkossa osoitteessa http://lib.tkk.fi/Diss/2008/isbn9789512295371/

Preface

The work reported in this thesis has been carried out in the Laboratory of physics at the Helsinki University of Technology during the years 2004-2008.

I wish to thank my advisor Docent Mikko Alava for his inspiring and active guidance during these years, without which completing this thesis would not have been possible. I would also like to thank Academy Professor Risto Nieminen for the possibility to work as a member of the COMP group, a well organized Center of Excellence established and lead by him. The work presented in this thesis has been done in fruitful collaboration with a number of people who I wish to thank: Prof. Stefano Zapperi, Prof. M.-Carmen Miguel, Dr. Paolo Moretti, Dr. Martin Rost and Dr. Martin Dubé. Special thanks belong to M.-Carmen Miguel for kind hospitality and interesting discussions during my two visits to University of Barcelona, as well as to Paolo Moretti for good company and for familiarizing me with the local culture. Stefano Zapperi is thanked for the possibility to visit the ISI Foundation in Turin. I thank Prof. Juhani von Boehm for collaboration in teaching. I also want to thank all the members of the Complex Systems and Materials group for interesting conversations and good atmosphere, including numerous evenings with the card game "Koira".

I am grateful to my family and especially to Jenni for encouraging and supporting me during this project.

Otaniemi, May 2008

Lasse Laurson

Contents

List of Publications

This thesis consists of an overview and of the following publications which are referred to in the text by their Roman numerals.

I L. Laurson, M.J. Alava, and S. Zapperi, "Power spectra of self-organized critical sandpiles", Journal of Statistical Mechanics: Theory and Experiment, L11001 (2005) (8 pages).

II M. Rost, L. Laurson, M. Dube, and M.J. Alava, "Fluctuations in fluid invasion into disordered media", Physical Review Letters, **98**, 054502 (2007) (4 pages).

III L. Laurson and M.J. Alava, "$1/f$ noise and avalanche scaling in plastic deformation", Physical Review E, **74**, 066106 (2006) (5 pages).

IV M.-C. Miguel, L. Laurson and M.J. Alava, "Material yielding and irreversible deformation mediated by dislocation motion", European Physical Journal B **64**, 443-450 (2008) (8 pages).

V P. Moretti, L. Laurson, and M.J. Alava, "Dislocation interactions mediated by grain boundaries", Journal of Statistical Mechanics: Theory and Experiment, P05010 (2008) (13 pages).

VI L. Laurson and M.J. Alava, "A Driven particle in a cloud of mobile impurities", Journal of Statistical Mechanics: Theory and Experiment, P07003 (2008) (10 pages).

Author's contribution

The author has had an active role in all phases of the research reported in this thesis. Most of the numerical calculations, data analysis and the related programming work were carried out by the author. The simulations of the phase field model in article **II** are due to Dr. Martin Rost, and some of the simulations presented in article **IV** have been performed by Prof. M.-Carmen Miguel. The analytical calculations in article **V** are mostly due to Dr. Paolo Moretti. The author has written articles **III** and **VI**, and contributed actively to the writing of the other papers.

1 On avalanches and noise in non-equilibrium systems

1.1 Introduction

Quite often, things in Nature do not happen smoothly. Instead, a typical response of a wide class of physical systems to slowly changing external conditions takes the form of a series of discrete events or *avalanches* spanning a broad range of sizes. Such "crackling noise" [1] is observed in several apparently very different systems, ranging from the sound emitted from a crumpling [2] or tearing [3] of a piece of paper to earthquakes occurring when slowly moving tectonic plates rub each other [4]. Other examples include Barkhausen noise (magnetic pulses emitted from a ferromagnet in a changing external field) [5, 6, 7] and motion of a fluid front when fluid invades porous media in an imbibition experiment [8, 9, 10]. Recent experimental evidence shows that also plastic deformation of crystalline solids is characterized by intermittent avalanches of plastic activity, contrary to the traditional picture of a smooth laminar flow process [11, 12, 13].

A common feature of these systems is that statistics of various measures associated to them - such as avalanche sizes and durations - appear to lack a characteristic scale. This scale invariance is reminiscent of what one observes at a critical point of a second order phase transition. Thus, such behaviour is often assumed to follow from the proximity of a *non-equilibrium phase transition* [14], or from mechanisms such as self-organized criticality (SOC) where the critical point is an attractor of the dynamics - the system self-organizes into a critical point without any apparent tuning of parameters [15].

To get more insight into this intriguing behaviour, numerical studies of such phe-

nomena using appropriately simplified model systems are of great importance. As systems exhibiting crackling noise are typically composed of a large number of interacting parts, a full model with all the microscopic details of a real system included would often be impossible to simulate with even the most powerful computers. Therefore a crucial feature of useful model systems is that they should be somehow simplified, but still preserve the essential properties of the original physical system. Such simplification (sometimes referred to as *coarse-graining*) of the system can be justified by the observation that systems with scale free or critical-like features typically also exhibit certain degree of *universality*: all the microscopic details are not important for the large scale behaviour of the system.

This thesis consists of studies of various simplified model systems exhibiting avalanche-like fluctuations and noise. The background and some central concepts related to crackling noise and avalanches are introduced in this Section. Sandpile models of self-organized criticality are studied in Section 2 to demonstrate that such simple models exhibit non-trivial temporal correlations, contrary to earlier claims. Similar findings are reported also for a phase field model of fluid invasion into disordered media (Section 3) as well as in the context of a simple dislocation dynamics model in Section 4. For the dislocation model, also other properties such as correlations between different avalanches, the history dependence of the dynamics, and the effect of grain boundaries on interaction between dislocations are considered. Finally, a study of a single particle interacting with mobile impurities is presented in Section 5.

1.2 Properties of crackling noise

A schematic example of a typical crackling noise signal $V(t)$ is shown in the upper panel of Fig. 1.1. Here it is assumed that $V(t)$ is a *stationary* signal (i.e. its statistical properties do not vary in time) characterizing the *global* behaviour of the

system, e.g. the total activity of some kind of a given system as a function of time t. There are two different methods that have been commonly used to characterize such a signal. One can either consider the signal as a collection of discrete bursts or avalanches and study the statistical properties of various measures associated to them, or view it as a noisy time series and study its spectral properties.

1.2.1 Avalanches

An avalanche is defined as a correlated and uninterrupted sequence of activity in a system composed of a large number of interacting constituents. Typically an avalanche is localized in space, but for systems in which the constituents interact through long range interactions this is not necessarily the case. To trigger an avalanche, some sort of perturbation needs to be applied to the system. This is achieved by driving the system from outside at a slow rate. In thermal systems, also thermal fluctuations can trigger avalanches. Such a perturbation can cause a small burst of activity somewhere in the system, which then may trigger further activity in its vicinity. In a critical system the characteristic size of such a chain reaction is limited only by the finite system size.

If the drive rate is sufficiently slow such that different avalanches do not overlap in time, one can study the avalanches simply by considering the global activity time series $V(t)$: a single burst in $V(t)$ corresponds to a single avalanche. However, identifying an avalanche from a time series such as that in Fig. 1.1 is often complicated by the fact that due to various reasons (e.g. experimental noise) one typically has a nonzero background in the signal $V(t)$ on top of which the bursts corresponding to avalanches can be observed. This background needs to be thresholded away in order to be able to define individual avalanches. As it is not *a priori* clear what would be the "correct" threshold value V_{th} to use, one needs to consider also the effect of varying the threshold.

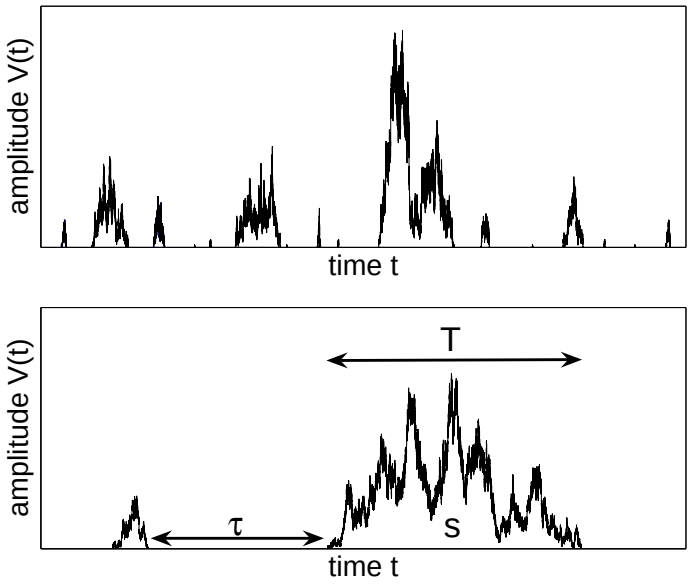

Figure 1.1: Top: A schematic example of a time series $V(t)$ consisting of distinct bursts, or avalanches. Bottom: A more detailed view from the beginning of the signal, showing definitions of the various quantities associated to the avalanches. The avalanche size s is the area under the part of the signal $V(t)$ corresponding to a single avalanche of duration T. The waiting time τ is here taken to be the quiet time interval between two successive avalanches, but other definitions such as the time interval between two consecutive avalanche triggerings are also possible.

Statistical properties of avalanches are usually studied by considering the probability distributions of various measures associated to them. These include the avalanche duration T and size s, defined by $s = \int_0^T [V(t) - V_{th}]dt$, see the lower panel of Fig. 1.1. Due to the lack of characteristic scale, the distributions can typically be described by power laws of the form

$$P(x) = x^{-\tau_x} f_c\left(\frac{x}{x_0}\right), \tag{1.1}$$

where τ_x is the exponent characterizing the statistics of the quantity $x = s, T, ...$, $f_c(z)$ is a scaling function satisfying $f_c(z) \to$ const. for $z \ll 1$ and $f_c(z) \to 0$ for $z \gg 1$. x_0 is a cut-off scale due to e.g. the finite system size.

In addition to the statistics of individual avalanches, correlations between different

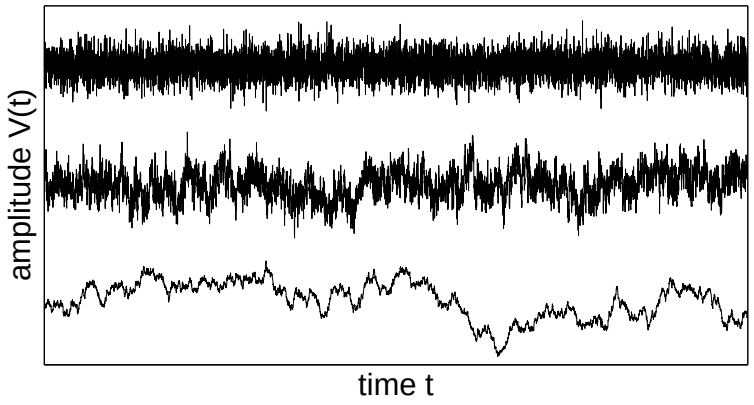

Figure 1.2: Examples of artificially generated noise signals. Top: Gaussian white noise, characterized by a flat power spectrum with $\alpha = 0$. Middle: $1/f$ noise with $\alpha = 1$. Bottom: Brownian noise (integrated white noise) with $\alpha = 2$.

avalanches are also of interest. If the triggerings of avalanches are uncorrelated, the *waiting times* τ (not to be confused with the exponent τ_x which in this thesis always appears with a subscript) between consecutive avalanches are expected to obey an exponential distribution. Quite often, however, a power law distribution for the waiting times is observed instead, indicating the presence of temporal correlations between triggerings of different avalanches [3, 16]. The tendency of avalanches to form clusters in time can in many cases be quantified by the Omori law, originally proposed in the context of earthquakes, stating that the event rate after the "main event" decays as a power law in time [17]. Similar conclusions have been made also for spatial correlations: avalanche locations within the system are not typically uniformly distributed: consecutive avalanches tend to be clustered in space [18].

1.2.2 Noise

Another possibility to characterize a stationary signal $V(t)$ is to regard is as "noise", and study its spectral properties by means of computing the power spectrum of

$V(t)$,

$$S(f) \sim \left| \int e^{i2\pi ft} V(t) dt \right|^2 . \tag{1.2}$$

An alternative definition of $S(f)$ is given by the Fourier transform of the correlation function $C(\theta) = \int V(t)V(t+\theta)dt$ of the stationary signal $V(t)$, $S(f) = \int C(t)e^{i2\pi ft}dt$. Typically also $S(f)$ assumes a power law form, scaling with frequency f as

$$S(f) \sim f^{-\alpha}, \tag{1.3}$$

where the value of the exponent α determines the type of noise. A crude classification is presented in Fig. 1.2. *White* or uncorrelated noise is characterized by a flat power spectrum with $\alpha = 0$, whereas a Lorentzian spectrum with $\alpha = 2$ corresponds to stationary *Brownian* noise, an example being the position of a random walker in a harmonic potential (i.e. the Ornstein-Uhlenbeck process) as a function of time. In between these two "trivial" cases, one has the interesting regime often referred to as $1/f$ noise, with $0 < \alpha < 2$. As this kind of noise is ubiquitous in Nature and also in some man-made systems, and has interesting properties such as long temporal correlations, a significant amount of activity has been devoted to trying to understand the origin of $1/f$ noise. One mechanism producing non-trivial $1/f$-like noise in a number of systems with avalanche dynamics over limited range of frequencies is presented below.

1.3 Scaling of the power spectrum

In the case of an avalanche-like time series $V(t)$, there exists a relation between the two approaches described above to characterize such a signal. It was originally proposed in the context of Barkhausen noise [23], and more recently it has been found to apply quite generally for systems exhibiting critical avalanche dynamics.

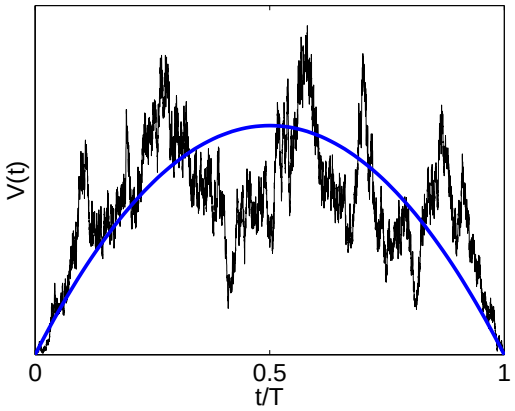

Figure 1.3: A schematic example of a part of the signal $V(t)$ corresponding to an individual avalanche (thin line with a rough shape) and the average avalanche shape, obtained by averaging over a large number of avalanches of given duration T (thick smooth line).

1.3.1 The average avalanche shape

Besides computing the distributions of simple avalanche properties such as their size and duration, also the more detailed structure of individual avalanches is of interest. Studies of e.g. the average *avalanche shape* provide another method to compare real physical systems with various simplified models [24], see Fig. 1.3

In a critical system one expects the avalanche shape to be independent of its duration, such that average avalanche shapes $\langle V(t,T)\rangle$ of avalanches of different durations T obey

$$\langle V(t,T)\rangle = T^{\gamma_{st}-1} f_{shape}(t/T), \tag{1.4}$$

where $f_{shape}(x)$ is a scaling function corresponding to the duration-independent average avalanche shape [23]. Notice that Eq. (1.4) contains also the scaling of the average avalanche size with the avalanche duration, $\langle s(T)\rangle \sim T^{\gamma_{st}}$. The exponent γ_{st} is related to the other avalanche exponents through $\gamma_{st} = (\tau_T - 1)/(\tau_s - 1)$ [14], a relation that can be easily derived by assuming a power law scaling of the form of

$\langle s(T)\rangle \sim T^{\gamma_{st}}$ and using $P(s)ds = P(T)dT$.

In simple model systems, avalanche shape is typically symmetrical, whereas in certain experimental systems, the observed avalanche shape displays some asymmetry. For Barkhausen noise, this has been demonstrated to be due to a negative effective mass of the moving domain walls arising from eddy current damping [25]. Also certain other experimental systems appear to exhibit some asymmetry in the avalanche shape [19], but it is not clear if the explanation proposed in [25] is applicable more generally.

1.3.2 Power spectra

Starting from Eq. (1.4), one may derive a relation between the power spectrum and avalanche scaling [23]. Consider first the probability $P(V|s)$ to get a certain value V in the $V(t)$-signal during an avalanche of size s. By assuming scaling and requiring normalization, one obtains $P(V|s) = V^{-1} f_V(V s^{1/\gamma_{st}-1})$, where $f_V(x)$ is a scaling function. Consequently, the avalanche energy $E(s)$ scales like

$$E(s) = \langle V^2\rangle s^{1/\gamma_{st}} = s^{1/\gamma_{st}} \int_0^\infty V^2 P(V|s) \sim s^{2-1/\gamma_{st}}. \tag{1.5}$$

The stationary time-time correlation function $C(\theta)$ is defined by

$$C(\theta) = \int V(t)V(t+\theta)dt. \tag{1.6}$$

By considering only the $V(t)$-signals corresponding to avalanches of size s in Eq. (1.6), one obtains the correlation function $C(\theta|s)$ for avalanches of a given size s. The $\theta = 0$ component of $C(\theta|s)$ is proportional to the avalanche energy $E(s)$. Thus, due to the scaling of $E(s)$ in Eq. (1.5), $C(\theta|s)$ scales like

$$C(\theta|s) = s^{2-1/\gamma_{st}} f_C(\theta s^{-1/\gamma_{st}}), \tag{1.7}$$

where $f_C(x)$ is a scaling function. The energy spectrum $E(f|s)$ of avalanches of a given size is then obtained as a cosine transform of $C(\theta|s)$,

$$E(f|s) = \int_0^\infty C(\theta|s)\cos(f\theta)\mathrm{d}\theta = s^2 g_E(f^{\gamma_{st}}s), \tag{1.8}$$

where $g_E(x)$ is a scaling function. To obtain the power spectrum $S(f)$ of the total signal, $E(f|s)$ is averaged over the avalanche size probability distribution, assumed to be a power law $P(s) \sim s^{-\tau_s}$ with a cut-off scale s^*. Thus,

$$S(f) = \int P(s)E(f|s)\mathrm{d}s = f^{-\gamma_{st}(3-\tau_s)} \int^{s^* f^{\gamma_{st}}} \mathrm{d}x x^{2-\tau_s} g_E(x). \tag{1.9}$$

By making the assumption that the avalanche dynamics is such that the elementary events forming an avalanche contribute to $E(f|s)$ only through local correlations, and that the local growth of an avalanche does not reflect the overall avalanche size, one has $E(f|s) \sim s$ [23]. This implies $g_E(x) \sim 1/x$, and one obtains from Eq. (1.9) for $\tau_s < 2$ the scaling

$$S(f) \sim f^{-\gamma_{st}}, \tag{1.10}$$

i.e. $\alpha = \gamma_{st}$ for frequencies $f > 1/T_0$, with T_0 the cut-off scale of the avalanche duration distribution. In the rare case with $\tau_s > 2$, the integral in Eq. (1.9) would converge and a scaling $\alpha = \gamma_{st}(3-\tau_s)$ ensues. The $\alpha = \gamma_{st}$ scaling has been found to be valid in a number of systems, including some of the ones discussed in this thesis [20, 21, 22]. As it is well known that the avalanche exponents (including γ_{st}) can assume non-trivial values, the above scaling relation gives a natural explanation to similar observations regarding power spectra of intermittent avalanche-like signals.

2 Sandpile models of self-organized criticality

In this Section power spectra of signals $V(t)$ consisting of avalanches in sandpile models of self-organized criticality are studied. In particular, it is shown that certain "classical" sandpile models exhibit activity time series $V(t)$ with non-trivial scaling of the power spectrum of $V(t)$. This contradicts earlier claims that such models should lead to to trivial Lorentzian power spectra. The results are published in article **I**.

2.1 Self-organized criticality

In 1987, Bak, Tang and Wiesenfeld (BTW) introduced a simple cellular automaton model to elucidate the concept of self-organized criticality (SOC), or as the authors put it in the title, "an explanation of $1/f$ noise" [15]. SOC is a mechanism through which a large class of slowly driven dissipative systems display scale free behaviour characteristic to a second order phase transition or a critical point, but without any apparent tuning of parameters. The general nature of the concept has lead to applications also outside the traditional realm of physics, and it has been proposed to be one of the mechanisms through which complexity arises in Nature [26].

2.2 Definition of the models

Sandpile models are model systems in which such ideas can be explored within a conveniently simple framework. After the introduction of the original model by BTW more than two decades ago, also a number of variants have been proposed. Here, we focus on two specific sandpile models, namely the original BTW-model

[15] and the stochastic Manna model [27].

These models are defined on a d-dimensional hypercubic lattice, with an integer variable z_i assigned on each lattice site i representing the number of "grains" present on that site. If for a given site the local variable reaches or exceeds a critical value z_c, the site *topples*, implying that some of the grains on that site are distributed among its nearest neighbours: $z_i \to z_i - z_c$ and $z_j \to z_j + 1$, where j denotes the nearest neighbour sites of the site i. The details of this toppling process determine the different models. In the deterministic BTW model, $z_c = 2d$ and each nearest neighbour of the toppling site will receive exactly one grain. The stochastic Manna model is defined by $z_c = 2$ and by a toppling process in which two randomly chosen nearest neighbours receive a grain.

The dynamics is typically chosen to be parallel, meaning that during a single time step all the sites are checked and those with $z_i \geq z_c$ will be toppled. A toppling can induce one of the neighbours of the toppling site to topple during the next time step, and so on. Such a chain reaction of topplings is an avalanche, with the size s defined as the total number of topplings and duration T as the number of parallel updates of the lattice during an avalanche.

Such systems are driven by adding new grains to the system at a slow rate to randomly chosen locations, $z_i \to z_i + 1$. Typically one implements the slow driving limit, in which new grains are added only when there is no activity. This driving is balanced by dissipation, which is usually implemented by choosing open boundary conditions such that if a boundary site topples, grains can leave the system through open boundaries.

By considering the above systems with periodic boundary conditions without any dissipation or drive (the so called fixed energy sandpile [28]), one finds a transition between active and inactive (often referred to as the absorbing state) phases when

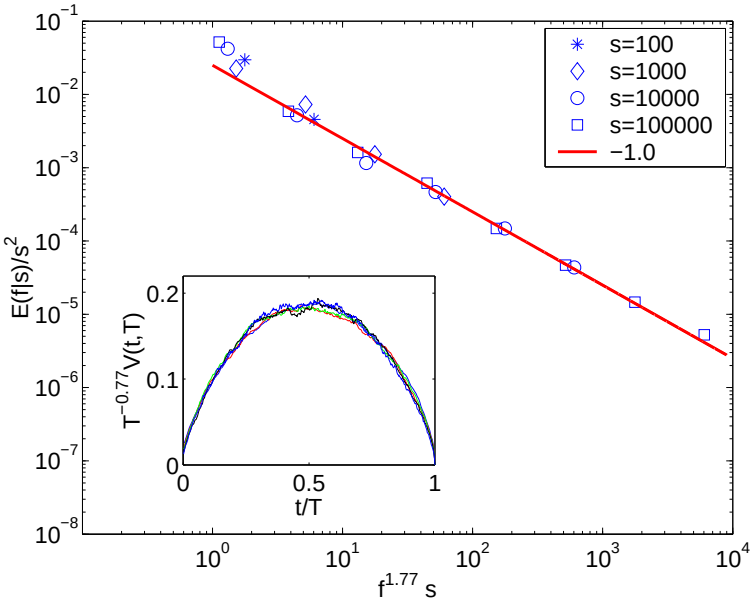

Figure 2.1: Main figure: The rescaled energy spectra of avalanches of size s, showing that the scaling function $g_E(x)$ decays as $1/x$. Inset: A data collapse showing the average avalanche shape for different T-values. Data from the 2d Manna model.

a control parameter, the grain density ζ is varied. The transition takes place at a specific critical value $\zeta = \zeta_c$ of the control parameter, and is characterized by scaling features typical for critical phenomena occurring at a second order phase transition. For instance the order parameter of the transition, the density of active sites ρ_a, behaves close to but above the critical point as $\rho \sim (\zeta - \zeta_c)^\beta$, where β is the associated critical exponent. Such models can also be mapped to models of interfaces moving in random media, consequently the absorbing phase transition can also be referred to as a depinning transition [29, 30].

The combination of the slow driving and dissipation present in the SOC version of the model drives the system towards the critical point of the absorbing/depinning transition. In the steady state, the grain density ζ of the SOC models fluctuates around the critical value ζ_c, and the model shows scale invariance with scaling exponents characteristic to the underlying absorbing/depinning transition [29, 30,

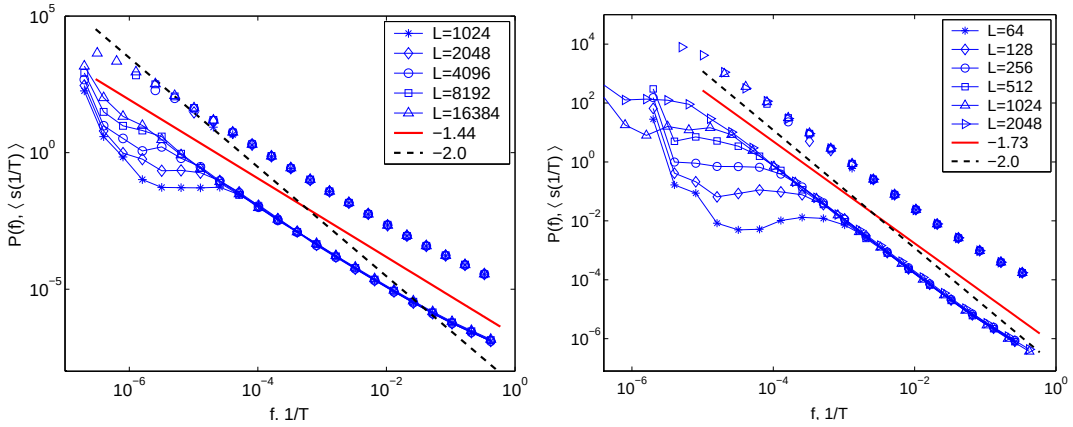

Figure 2.2: Power spectra (symbols connected by a line) and average avalanche size as a function of the inverse avalanche duration (symbols without a connecting line). Left: Manna $d = 1$. Right: Manna $d = 2$.

31]. E.g. the avalanche size distributions can be characterized by power laws of the form

$$P(f) = s^{-\tau_s} f_c(s/s_0), \tag{2.1}$$

with the cut-off scale s_0 scaling with the linear system size L as $s_0 \sim L_s^D$.

2.3 Power spectra

An important issue in the context of the sandpile models of SOC is the possible existence of complex temporal correlation in the activity time series extracted from such simple models. Most often this is studied by computing the power spectrum of a time series $V(t)$, which could be for instance the number of topplings as a function of time, with one parallel update of the lattice defining the unit of time. The system is driven slowly with an uncorrelated driving such that different avalanches do not overlap in time. The history of such studies has been confusing: First, BTW claimed that the sandpile model gives rise to a $1/f$-type power spectrum of $V(t)$,

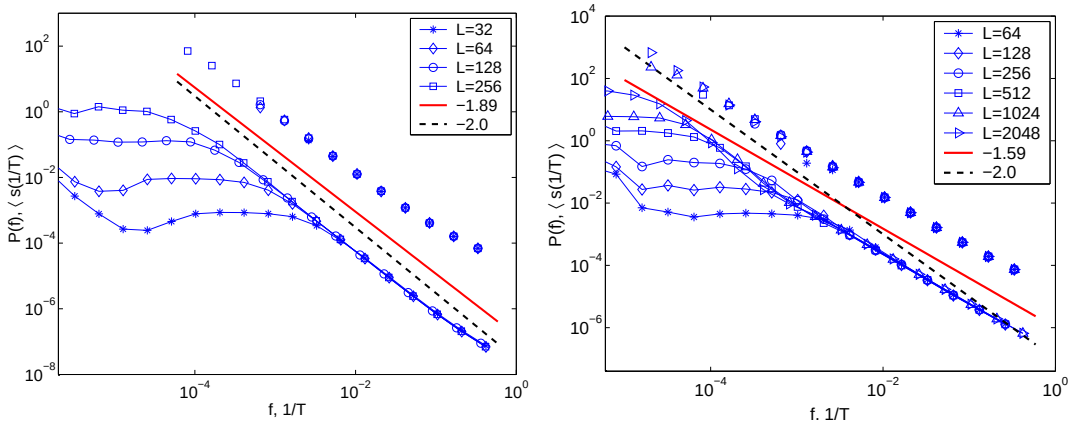

Figure 2.3: Power spectra (symbols connected by a line) and average avalanche size as a function of the inverse avalanche duration (symbols without a connecting line). Left: Manna $d = 3$. Right: BTW $d = 2$.

with the exponent α close to 1 [15]. Soon after that, two groups published results indicating that sandpile models should instead lead to Lorentzian power spectra, with $\alpha = 2$ [33, 34]. After that, a number of different versions of the original sandpile model have been proposed, some of them apparently displaying non-trivial temporal correlations or $1/f$-like power spectra [35, 36, 37, 38]. But, in article **I**, it is shown that the original BTW model and the stochastic Manna model, without any modification, follow the apparently generic scaling of the power spectrum, Eq. (1.10), with $\alpha = \gamma_{st}$, thus giving rise to non-trivial scaling of the (high frequency) power spectrum. These results are not sensitive to the drive rate (i.e. the quiet times between avalanches), as long as it is slow enough such that different avalanches do not overlap in time.

To demonstrate how this result arises from the generic derivation presented in Section 1, the energy spectrum of avalanches as well as the average avalanche shapes are computed. For the 2d Manna model, the scaling of the energy spectrum $E(f|s)$ is observed to be consistent with $g_E(x) \sim 1/x$, and the average avalanche shape is found to be symmetrical and obey Eq. (1.4), see Fig. 2.1. For the BTW model, com-

plications arise as the avalanches appear to develop an asymmetry varying slowly with the avalanche duration T. Such observations could be related to the multiscaling that the BTW model has been found to exhibit [32]. Nevertheless, the Manna model in d = 1,2 and 3 as well as the $d = 2$ BTW model all appear to obey the scaling $\alpha = \gamma_{st}$, with $\alpha = \gamma_{st} \approx 1.44, 1.77$ and 1.9 for the Manna model in $d = 1, 2$ and 3, respectively, and $\alpha = \gamma_{st} \approx 1.59$ for the BTW model with $d = 2$. For $d \geq 4$, with $d = d_c = 4$ the upper critical dimension of the models at hand, mean field exponents are expected, implying $\alpha = \gamma_{st} = 2$.

This finding contradicts earlier claims that such models should lead to Lorentzian power spectra independent of the model details and spatial dimension d [33, 34]. Instead, in the physically interesting dimensions $d < d_c = 4$, non-trivial scaling of the high frequency power spectrum is observed, with the value of the exponent α reflecting the universality class of the underlying avalanche dynamics. One should note, however, that the above applies only for frequencies higher than that corresponding to the inverse duration $1/T_0$ of the longest avalanche in the system. $1/f$ noise arising from correlations between different avalanches, as apparently observed in a number of systems, remains to be explained.

3 Fluctuations in fluid invasion into disordered media

Another example system involving avalanche dynamics, the dynamics of a fluid front invading disordered porous media is considered in this Section. By studying the phase field model of the problem, it is shown that the avalanche-like propagation of the front gives rise to a fluctuating spatially averaged interface velocity, obeying the generic scaling of the power spectrum, Eq. (1.10). Furthermore, the scaling of the velocity fluctuations of the advancing fluid front with the mean velocity is investigated and compared to interfaces moving in random media without a conservation law. The results are reported in more detail in article **II**.

3.1 Fluid invasion into disordered media

The process of a viscous fluid displacing air or a less viscous fluid in disordered porous media constitutes an important problem, with many applications in various fields of engineering and technology, ranging from oil industry applications [39] to ink penetration in paper in printing processes [40]. A more familiar example from everyday life of such an *imbibition* experiment could be a napkin that is accidentally put in contact with a cup of coffee. Due to capillary forces arising from the porous structure of the medium (napkin), the fluid (coffee) is sucked from the reservoir (cup), and an interface separating the invaded (wet) and noninvaded (dry) regions propagates. Due to the disordered structure of the medium, such an interface is typically observed to be rough.

In more controlled experiments, such phenomena have been demonstrated to exhibit robust scaling features. In *spontaneous imbibition*, such as the above example

involving napkin and coffee, the average interface height $\bar{h}$ grows in time according to the Washburn's law $\bar{h} \sim t^{1/2}$ [41]. *Forced flow imbibition* arises if the pressure at the liquid reservoir is increased as the interface advances, by keeping the mean pressure gradient $|\nabla P| = (P_R - P_I)/\bar{h}$ constant, where P_R and P_I are the pressures at the reservoir and interface, respectively. In general, the fluid interface advances as fluid is transported from the reservoir through the medium. Such a fluid flow obeys Darcy's law,

$$\vec{i} = -\frac{\kappa}{\eta}\nabla P, \tag{3.1}$$

where the flux $\vec{i}$ arises due to a pressure gradient ∇P, with η the viscosity of the liquid and κ the permeability of the medium [42]. The pressure P_I at the interface is a superposition $P_I = \gamma^*\mathcal{K} + P_c + P_0$ of the effect of coarse-grained curvature $\mathcal{K}$ by an effective interface tension γ^*, the capillary (P_c) and atmospheric (P_0) pressures.

The porous structure of the medium gives rise to two different kinds of quenched disorder: The capillary disorder $p_c(\vec{r}) = P_c + \delta p_c(\vec{r})$ acting only at the interface, and permeability disorder $\kappa(\vec{r}) = \kappa + \delta\kappa(\vec{r})$ affecting the flux of liquid from the reservoir towards the interface. Consequently, one can identify two different length scales. Due to the tendency of the effective (capillary) interface tension and the average pressure gradient to smoothen the interface, correlated roughness can be observed only up to a lateral length scale

$$\xi_c \sim \sqrt{\frac{\kappa\gamma^*}{\eta\bar{v}}} = \sqrt{\frac{\kappa}{\mathrm{Ca}}}, \tag{3.2}$$

where $\mathrm{Ca} = \eta\bar{v}/\gamma^*$ is the capillary number [43]. Another length scale due to the ratio of the disorder strengths [44] is given by

$$\xi_\kappa \sim \frac{\kappa^2}{\bar{v}\eta}\frac{\delta p_c}{\delta\kappa} = \frac{\sqrt{\kappa}}{\mathrm{Ca}}. \tag{3.3}$$

Thus, for the case of a slowly advancing front (or low Ca), one has $\xi_\kappa > \xi_c$ and capillary-induced fluctuations prevail.

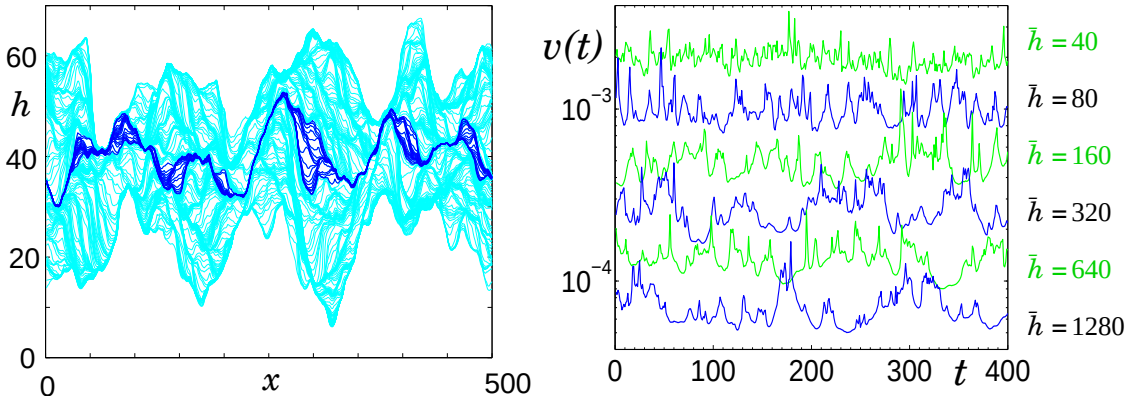

Figure 3.1: Left: Interface configurations $h(x,t)$ for $L = 500$ and $\bar{h} = 320$. Two consecutive configurations have a time separations of 500 time units. Right: Time series $v(t)$ for various values of $L = \bar{h}$.

3.2 Phase field model

To model the imbibition process, a phase field model of the problem is considered [43]. An energy functional

$$\mathcal{F}[\phi] = \int d^{d+1}r \left[\frac{(\nabla\phi)^2}{2} - \frac{\phi^2}{2} + \frac{\phi^4}{4} - \alpha\vec{r}\phi \right] \tag{3.4}$$

couples a scalar phase field $\phi(\vec{r},t)$ to quenched randomness $\alpha(\vec{r})$ characterized by the mean value $\bar{\alpha} > 0$ and standard deviation $\Delta\alpha$, modelling capillary disorder. The invaded and non-invaded regions correspond to $\phi = 1$ and $\phi = -1$, respectively. The model is defined in the $d+1$ -dimensional half-space, $\vec{r} = (\vec{x}, y)$, with $y > 0$. As the system is coupled to a liquid reservoir at the bottom, the appropriate boundary condition is $\phi = 1$ at $y = 0$. The initial condition for the simulations is chosen to be a dry system with $\phi(\vec{r}, t = 0) = -1$.

The dynamics in such a system is due to the chemical potential, or pressure, $\mu = \delta\mathcal{F}/\delta\phi$, which drives the current $\vec{j} = -\tilde{\kappa}\nabla\mu$. As liquid is conserved in the flow process, the appropriate dynamical equation for ϕ assumes the form of the continuity

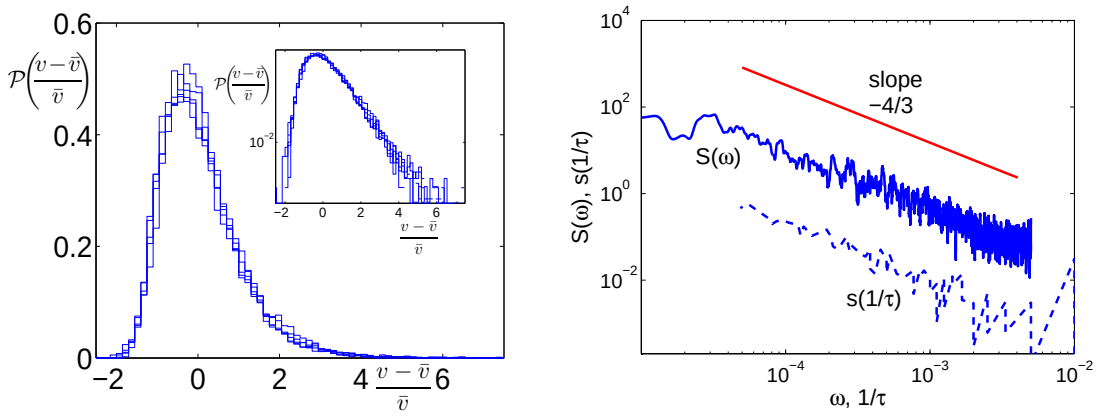

Figure 3.2: Left: Scaled velocity distributions for various values of $\bar{h} = L$ Right: Power spectrum of $v(t)$ for $L = \bar{h} = 1280$, and the avalanche size $s(1/T)$ as a function of the inverse duration $1/T$.

equation,

$$\partial_t \phi = -\nabla \cdot \tilde{\kappa}(\vec{r}) \nabla \left[\nabla^2 \phi + \phi - \phi^3 + \alpha(\vec{r}) \right]. \tag{3.5}$$

Numerical simulations of the model mimicking forced flow imbibition are performed by continuously shifting the space-dependent fields $\phi(\vec{r}, t)$, $\tilde{\kappa}(\vec{r})$ and $\alpha(\vec{r})$ downward with velocity $\bar{v}$. In the steady state this keeps the average interface height $\bar{h}$ constant at $\bar{h} = \bar{\alpha}/(2\bar{v})$ [43].

3.3 Fluctuations of the fluid front

To study the fluctuations of the interface velocity, the case of a slowly propagating interface is considered, such that $\xi_\kappa > \xi_c$. In this limit the capillary disorder dominates and permeability noise can be ignored. Thus, in the simulations only capillary disorder is considered, by setting $\kappa(\vec{r}) = \kappa$ in Eq. (3.5).

The propagation of the rough interface is observed to take place in a sequence of avalanches or localized bursts of fast interface motion. Such fast moving parts of the interface are surrounded by non-propagating or pinned regions arising from liquid conservation: liquid is being dragged from a surrounding region of lateral size $\bar{h}^d$ to allow the interface to propagate in the fast moving part of the interface. These fast moving parts can be identified with regions of maximal capillary forces experienced by the interface. At some point this moving part will encounter lower capillary forces and get pinned. Then, another part of the interface will start moving.

Such dynamics gives rise to a spatially averaged velocity $v(t)$ of the interface, which in the limit of slow imposed $\bar{v}$ (or high $\bar{h}$) becomes increasingly intermittent, see Fig. 3.1. For $\bar{h} \geq L$, there is typically only one avalanche going on in the system at any given time, so that bursts in $v(t)$ can be related to individual localized avalanches. In the left panel of Fig. 3.2, distributions $P(v)$ of the spatially averaged interface velocity are shown. These resemble Gumbel distributions of extreme value statistics, reflecting the fact that avalanches are occurring in regions of maximal capillary pressure. The size or volume of such avalanches is expected to scale with the duration as $s(T) \sim T^{\gamma_{st}}$. If an avalanche has a lateral size l, then its vertical extent is given by $w \sim l^{\chi_{loc}}$, where χ_{loc} is the local roughness exponent. The avalanche size is then given by $s \sim l^{d+\chi_{loc}}$. The scaling of avalanche durations with l is obtained by noticing that an avalanche takes place in a region of higher capillary forces than in other parts of the interface. Due to the independence of the local values of p_c, the excess velocity is related to l like $v \sim l^{d/2}$, implying $T = w/v \sim l^{\chi_{loc}+d/2}$. Thus, a relation $s(T) \sim T^{\gamma_{st}}$ with

$$\gamma_{st} = \frac{\chi_{loc} + d}{\chi_{loc} + d/2} \tag{3.6}$$

is obtained. For the case at hand, with $d = 1$, one has $\chi_{loc} = 1$ and consequently $\gamma_{st} = 4/3$. Due to the relation (1.10), one thus expects that also the high frequency part of the power spectrum $S(f) = \langle |\hat{v}(f)|^2 \rangle$ of $v(t)$ for the interface with $d = 1$ scales like $S(f) \sim f^{-4/3}$. Numerical results consistent with this are presented in the right panel of Fig. 3.2.

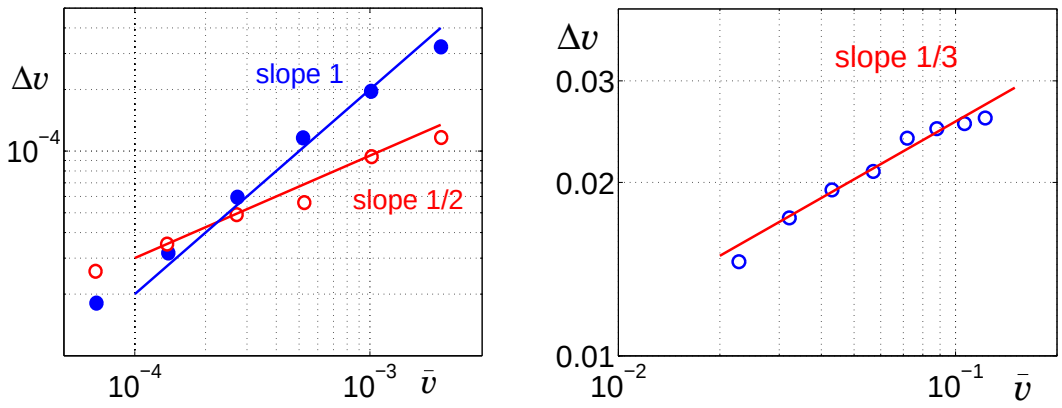

Figure 3.3: Left: Fluctuations Δv as a function of the mean velocity $\bar{v}$, for a constant $L = 500$ (open circles) and for $L = \bar{h}$. Right: Δv vs. $\bar{v}$ for the local model, $L = 10^4$.

Let us next consider the relation between the mean interface velocity $\bar{v}$ and the fluctuation Δv. The overall average velocity of the interface is related to the average avalanche velocity $\bar{v}_{ava}$ trough $\bar{v} \approx (\xi/\bar{h})^d \bar{v}_{ava}$, where $\xi = \xi_c$ or ξ_κ, giving the cut-off length scale of the moving avalanches. Within a region of lateral size $\bar{h}$, the overall velocity fluctuation is given by $(\xi/\bar{h})^d \Delta v_{ava}$. As there are $(L/\bar{h})^d$ such independent regions,

$$\Delta v \sim \left(\frac{\bar{h}}{L}\right)^{d/2} \left(\frac{\xi}{\bar{h}}\right)^d \Delta v_{ava}. \tag{3.7}$$

By further assuming that the avalanche velocity fluctuations obey $\Delta v_{ava} \sim \bar{v}_{ava}$, one gets

$$\Delta v \sim \left(\frac{\bar{h}}{L}\right)^{d/2} \bar{v}. \tag{3.8}$$

Due to $\bar{v} \sim 1/\bar{h}$, this gives rise to

$$\Delta v \sim \bar{v}^{1-d/2} L^{-d/2}. \tag{3.9}$$

The left panel of Fig. 3.3 shows the relation Δv vs. $\bar{v}$ for two different geometries, and a reasonable agreement with predictions of Eqs. (3.8) and (3.3) is found.

This can be compared with the velocity fluctuations of an interface without any conservation law, driven by a force F through a random medium. In such a situation, there typically exists a zero temperature critical value F_c for the driving force, separating pinned and propagating states. In the vicinity of such a depinning transition, a diverging correlation length $\xi \sim (F - F_c)^{-\nu}$ and order parameter scaling of the form $\bar{v} \sim (F - F_c)^{\theta}$ ensues. In the critical region where $\xi \approx L$, θ assumes a non-trivial value less than 1, while for slightly larger driving forces one has $L > \xi$ and a cross-over to $\bar{v} \sim (F - F_c)$ takes place.

In a system of lateral size L, one has $N = (L/\xi)^d$ independent subvolumes. The local spatially averaged velocities within these subvolumes are then independent random variables with mean $\bar{v}$ and standard deviation assumed to obey $\delta v \sim \bar{v}$. The fluctuations of the overall instantaneous velocity are then given by

$$\Delta v \sim \delta v/\sqrt{N} \sim \bar{v}^{1-d\nu/(2\theta)} L^{-d/2}. \tag{3.10}$$

Numerical simulations with the cellular automaton version of the $d = 1$ quenched Edwards-Wilkinson equation $\partial h/\partial t = \Gamma \nabla^2 h + F + \eta(x, h(x,t))$ (with η an uncorrelated quenched noise) in the regime with $L/\xi = O(10)$ are in reasonable agreement with Eq. (3.10), yielding $1 - d\nu/(2\theta) = 1/3$ by using an effective $\theta_{eff} = 1$ and $\nu = 4/3$, the known critical value for the $d = 1$ depinning transition, see the right panel of Fig. 3.3. Thus, the character of the velocity fluctuations of a driven interface depend on the presence or absence of a conservation law.

4 Discrete dislocation dynamics

Let us next consider the rich phenomenology arising from dynamics of interacting dislocations, line-like defects present in crystalline solids. The results regarding the relation (1.10) between avalanches of dislocation activity and noise in such systems have been published in article **III**. Article **IV** deals with apparent temporal correlations between distinct avalanches and the dependence of such correlations on the thresholding procedure applied to identify avalanches. Also the history dependence of the dynamics is studied. The results on a low angle grain boundary interacting with a single edge dislocation are published in article **V**.

4.1 Plastic deformation of solids

Plastic deformation of crystalline solids has been an active field of study already for a long time due to its enormous practical importance for various engineering applications. It is well established that the dominating contribution of irreversible deformation arises from the nucleation and motion of dislocations, linear defects of the ordered crystal lattice. The traditional picture of the deformation process has been that of a smooth laminar flow -like process in which fluctuations average out when large enough scales are considered. However, recent experimental observations have challenged this paradigm: Instead, plastic deformation of crystalline [11, 12, 13, 45, 46, 47, 48] as well as amorphous [49, 50, 51] solids is characterized by intermittent avalanches of plastic activity spanning several orders of magnitude in size. Similar results have been obtained also by modelling the plastic deformation of crystalline solids by means of discrete dislocation dynamics models of varying degree of complexity, ranging from simple two dimensional models involving point-like dislocations [52] to more realistic three dimensional simulations with flexible dislocation lines [53].

4.2 Morphology of crystalline solids

Crystalline solids are ordered structures formed by the constituent atoms of the material. These can have different structures (such as BCC, FCC) depending on the material at hand. However, real crystals are usually not perfect. Instead, a typical piece of solid material with crystalline structure contains a finite concentration of various defects, including point defects such as vacancies, interstitial and substitutional atoms, as well as line defects such as dislocations. On larger scales, crystalline materials are often composed of distinct grains with a specific crystallographic orientation in each grain, separated from each other by planar defects called grain boundaries.

Dislocations are the defects the motion of which is typically responsible for the majority of the plastic deformation of crystalline solids. Two specific kinds of dislocations are the edge dislocation and the screw dislocation, see Fig. 4.1 for a schematic illustration of the former. Also mixed dislocations combining aspects of both types are common. Dislocations can be characterized by a "topological charge", the Burgers vector $\vec{b}$, indicating the magnitude and direction of the induced lattice distortion.

Under an applied external (shear) stress, dislocations tend to move, or glide, in some specific slip planes containing both the dislocation and its Burgers vector, defined by the underlying crystal structure. Slip motion of a screw dislocation is possible in any plane containing the dislocation, as the dislocation and its Burgers vector are parallel. The Burgers vector of an edge dislocation is perpendicular to the dislocation line, implying that for a given edge dislocation there is only one plane in which it can move by glide. Another mechanism contributing to dislocation motion is called climb, through which an edge dislocation can move perpendicular to its slip plane. As dislocation climb is due to diffusion of vacancies, it is a strongly temperature dependent phenomenon. For low temperatures, dislocation glide is the

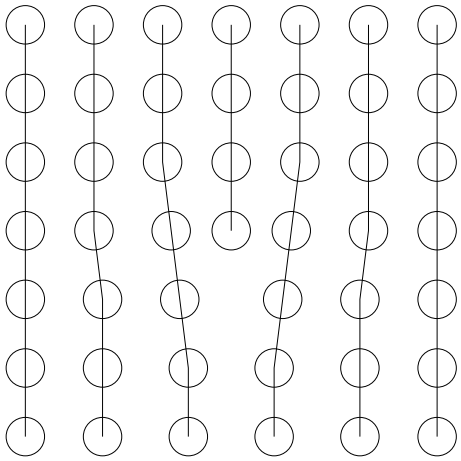

Figure 4.1: A schematic diagram of an edge dislocation. The dislocation line is located where the extra plane of atoms inside the crystal ends.

dominating mechanism for motion of edge dislocations.

4.3 Discrete dislocation dynamics model

A common feature of a class of models referred to as discrete dislocation dynamics (DDD) models is that there the dislocations are taken as the fundamental entities of the model, instead of the atoms of the underlying lattice [52, 53, 54, 55]. Such an approach is convenient as unlike in atomistic simulations [56] it makes it possible to study systems with reasonably large number of dislocations, but at the same time allows a more detailed description of individual dislocation processes than various continuum models where dislocation densities are considered to be the basic variables [57, 58, 59].

Here, a simple two-dimensional discrete dislocation dynamics (DDD) model similar to the one presented in Ref. [52] is considered. The point-like dislocations are assumed to be of edge type, and they can also be thought to represent cross-sections

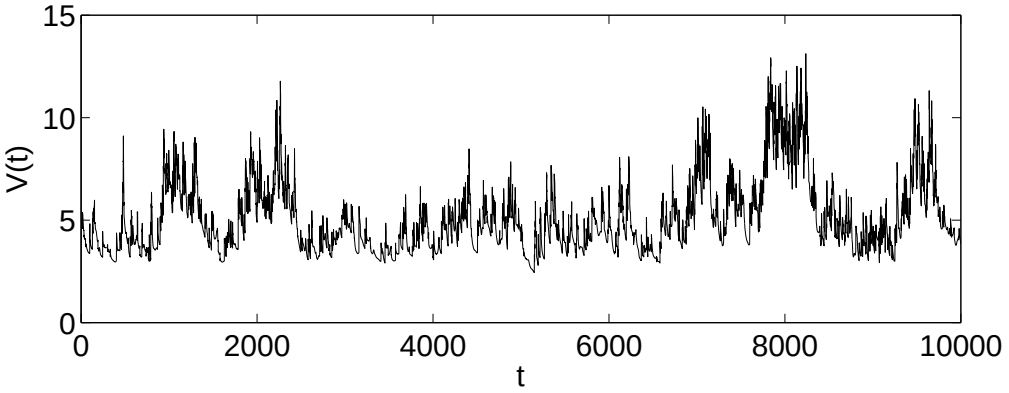

Figure 4.2: An example of a time series $V(t) = \sum_i |v_i|$, showing bursts of dislocation activity.

of straight dislocations in a three dimensional system. For simplicity only dislocation glide along a single slip direction parallel to their Burgers vectors $\vec{b} = \pm b u_x$ is considered. The equations of motion are assumed to be overdamped, with the velocity of the n'th dislocation v_n given by

$$\frac{\chi_d^{-1} v_n}{b} = b s_n \left[\sum_{m \neq n} s_m \sigma_s(\vec{r}_{nm}) + \sigma \right], \tag{4.1}$$

where v_n is the velocity of the nth dislocation, χ_d is the dislocation mobility, s_n refers to the sign of the Burgers vector of the nth dislocation, and σ is the external shear stress acting on the dislocations. The dislocations interact with each other through their long range elastic stress fields of the form

$$\sigma_s(\vec{r}) = \frac{\mu b}{2\pi(1-\nu)} \frac{x(x^2-y^2)}{(x^2+y^2)^2}, \tag{4.2}$$

with μ the shear modulus and ν the Poisson ratio of the material. Dimensionless versions of the equations of motion (4.1) are studied by measuring lengths in units of b, times in units of $1/(\chi_d D b)$ and stresses in units of $\mu/[2\pi(1-\nu)]$. Phenomenological annihilation and multiplication reaction are also implemented: If the distance between two dislocations with Burgers vectors of opposite signs is less than $2b$, they are removed from the system. This is balanced by monitoring the local stress in the

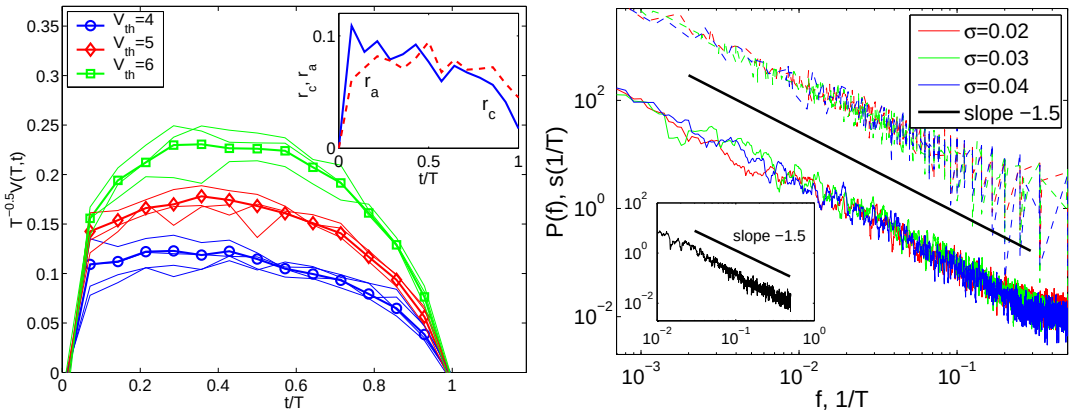

Figure 4.3: Left: The average avalanche shape for different threshold values V_{th}. The inset shows the average creation and annihilation rates (r_c and r_a, respectively) during an avalanche. Right: Power spectra of the signal $V(t) = \sum_i |v_i|$ (dashed lines) and the avalanche size (solid lines) as a function of the inverse duration, for various values of the external stress σ. The inset shows an example of the power spectrum of the strain rate signal.

system and adding a new dislocation pair to the system with a probability proportional to the local stress magnitude if it exceeds some threshold value. This is done in such a way that the local stress magnitude will decrease due to the stress field of the new dislocation pair, mimicking the effect of dislocation multiplication through Frank-Read sources in real plastically deforming crystals [60].

4.4 Noise and avalanches

Such a system has been demonstrated to undergo a transition between a *jammed* and moving steady states, as the control parameter, the external stress σ is increased. Close to the transition point, $\sigma = \sigma_c$, the strain rate

$$\dot{\gamma} = \frac{b}{L^2} \sum_i b_i v_i \tag{4.3}$$

exhibits power law time dependence $\dot{\gamma} \sim t^{-\theta}$ for the early times, with $\theta \approx 2/3$, reminiscent of the Andrade creep law observed in a number of systems ranging from metals [61] to paper [62]. For $\sigma < \sigma_c$, the system will eventually get stuck, due to the self-induced constraints on dislocation motion arising from the combination of long range elastic interactions and kinematical constraints due to the single slip geometry considered. For $\sigma > \sigma_c$, however, a moving steady state is observed after the initial transient. This state is characterized by large fluctuations of dislocation activity, visible as burst in the collective velocity signal

$$V(t) = \sum_i |v_i|. \tag{4.4}$$

The sizes $s = \int_0^T [V(t) - V_{th}]$ of such avalanches have been found to exhibit power law scaling, with an exponent τ_s close to $\tau_s = 1.6$ [52].

More detailed studies reveal that the shape of these avalanches appears to be slightly asymmetrical in time, see the left panel of Fig. 4.3. While this is in agreement with experimental observations regarding the pulse shape in acoustic emission studies [19], it could also arise from the way dislocation multiplication is implemented. The instantaneous introduction of a dislocation pair changes the stress field in the system in a discontinuous way, thus causing a jump in the collective velocity signal $V(t)$. As such a multiplication event is one of the microscopic processes contributing to an avalanche, it could explain some of the observed asymmetry.

Furthermore, avalanches are observed to follow the scaling $\langle s(T) \rangle \sim T^{\gamma_{st}}$ with $\gamma_{st} \approx 1.5$, independent of the threshold value V_{th}. This is in reasonable agreement with the previous results for the model, as can be seen by the scaling relation

$$\gamma_{st} = \frac{2\tau_E - 2}{2\tau_E - \tau_s - 1}, \tag{4.5}$$

yielding $\gamma_{st} \approx 1.6$ by using $\tau_s = 1.6$ [52] and $\tau_E = 1.8$ (with τ_E characterizing the statistics of the quantity $E = (\sum_i |v_i|)^2$ [12]). Similar conclusions apply to the power spectrum of the signal $V(t)$, which scales as $S(f) \sim f^{-\alpha}$, with $\alpha \approx 1.5$, see the right panel of Fig. 4.3. Thus, the relation $\alpha = \gamma_{st}$ is satisfied also in this case.

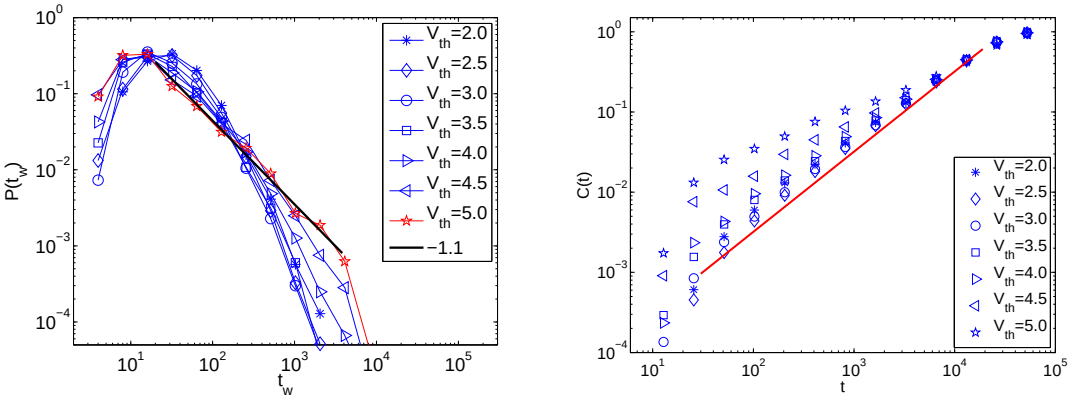

Figure 4.4: The effect of the threshold value V_{th} on the observed correlations between avalanches. Left: Distributions of the waiting times τ, defined to be the time interval between the starting times of two consecutive avalanches. Right: The correlation integrals of avalanche starting times.

4.5 Correlations between different avalanches

In a number of experimental systems with avalanche dynamics, temporal correlations of different avalanches are often observed [3, 16]. Typically this happens through clustering of avalanches, the best known example being aftershocks in the context of earthquakes, with their statistics being described by the Omori law [17]. An often used technique to check if such correlations exist is to study the waiting time distribution between avalanches. For uncorrelated avalanche triggerings, one expects an exponential distribution of waiting times, and consequently deviations from this simple form are often interpreted to indicate the presence of some correlations between avalanche triggerings. Another possibility is to analyze the correlation integral of avalanche starting times [45].

In the present case one has to threshold the signal with some threshold value V_{th} in order to be able to define individual avalanches. Thus, also the effect of varying the threshold needs to be considered. The waiting times are here defined to be the time

intervals between the starting times of two consecutive avalanches. Their distribution is observed to evolve with the threshold, such that for low V_{th}-values the forms of the distributions are close to exponentials, whereas for higher threshold values a cross over to a power law distribution with an exponent $\tau_\tau \approx 1$ is observed, see the left panel of Fig. 4.4. Similar conclusions can be made based on the correlation integrals of the avalanche starting times, right panel of Fig. 4.4: For low thresholds, the starting times appear to be almost random, whereas for higher threshold values significant clustering is observed.

This can be interpreted to arise from the breaking of individual avalanches into correlated subavalanches as the imposed threshold value is increased: An avalanche, by definition, is a correlated sequence of activity, and thus different parts of the same avalanche are correlated. While it is unclear to what extent such an idea might explain the apparent avalanche clustering observed in various experiments, it could be worth considering in more detail in the future.

4.6 History dependent dynamics

Dislocation ensembles have been proposed to belong to a family of glassy systems, characterized by slow dynamics and ageing. Such issues have previously been studied in the absence of externally applied stresses, by studying the relaxation of random dislocation configurations [63]. Recent experiments have addressed also the effect of an applied stress [64]. Here, the waiting time dependent response of the system is discussed briefly in the case where an external stress is applied, in the form of various cyclic loading/unloading histories subject to the dislocation ensemble.

The left panel of Fig. 4.5 shows an example of such a situation, with a stress close to σ_c applied for three cycles, separated from each other by waiting times of equal duration $\tau = 5 \times 10^3$ time units during which no stress is applied. The first loading

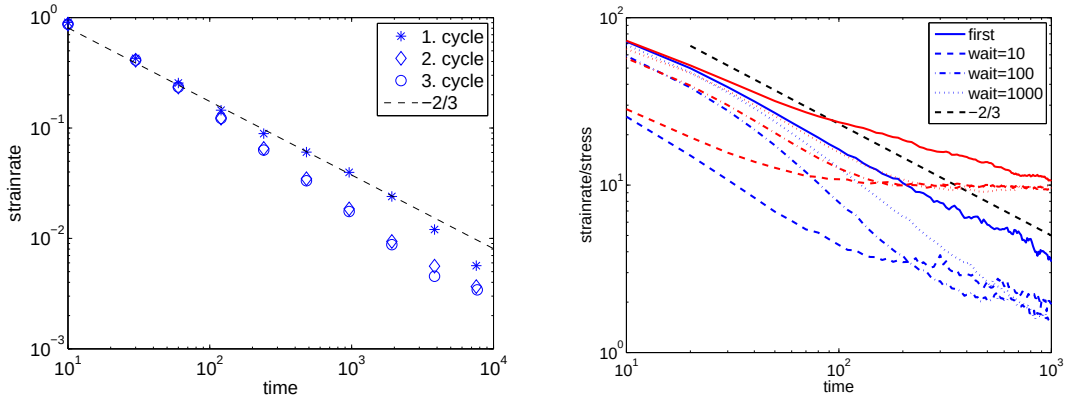

Figure 4.5: Time evolution of the average strain rate in loading/unloading cycles with constant stress during the loading steps. Left: $\sigma = 0.01$, unloading cycles of equal duration $\tau = 5 \times 10^3$. Right: Two different stress values ($\sigma = 0.01$ for the blue curves, $\sigma = 0.04$ for the red curves) and unloading cycles of different durations $\tau = 10, 10^2, 10^3$.

cycle reproduces the Andrade creep scaling $\dot{\gamma} \sim t^{-2/3}$, but the last two do not: the system appears to be "stronger" after the initial loading cycle - the strain rate decays faster in time. The right panel of Fig 4.5 shows similar cyclic simulations for two external stress values, but with different waiting times ($\tau = 10, 10^2, 10^3$) between the loading steps. Both the initial regime of slow relaxation as well as the crossover time to the steady state are observed to depend clearly on the loading history. This non-trivial response of the system needs to be further explored in the future.

4.7 On the effect of grain boundaries

The scale free dynamics of plastic deformation of crystalline solids described above in the case of single crystals is nowadays a well established phenomenon. However, less is known about the intermittent dynamics of plastic deformation of solids with polycrystalline structure. Recent experiments on polycrystalline ice samples indicate

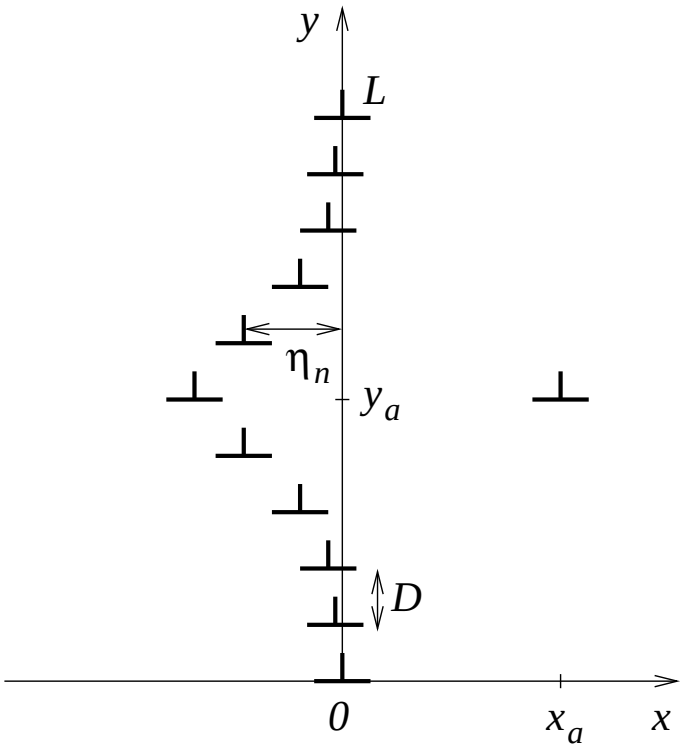

Figure 4.6: A schematic figure of the grain boundary dislocation system.

that the characteristic scale due to the average grain size $\langle d \rangle$ induces a $\langle d \rangle$-dependent cut-off to the distribution of acoustic emission amplitudes [65]. Also the power law exponent appears to change from the single crystal case [65]. Other effects of the polycrystalline structure include the so called Hall-Petch law, relating the yield strength of the material to the grain size [66].

To understand such phenomena, a crucial question is the effect of grain boundaries on the propagation of the avalanches of plastic activity from one grain to the other. In the following, as a conveniently simple starting point for such considerations, the interaction of a single dislocation with a deformable low-angle grain boundary is studied.

The low angle grain boundary is schematized as a linear assembly of $N + 1$ edge

dislocations distributed along the y-direction with a constant spacing D, with Burgers vectors $\vec{b}$ parallel to x axis. The grain boundary is taken to be pinned at both ends ($y = 0$, $y = L$), but can otherwise be deformed under an applied shear stress. Such deformations are denoted by a vector $\vec{\eta}$, with η_n the displacement of the nth dislocation along the x axis, see Fig. 4.6. Then, up to quadratic terms in η_n, the energy cost of deformation reads

$$E[\eta] = \frac{K}{2} \sum_{m \neq n} \frac{(\eta_m - \eta_n)^2}{(m-n)^2}, \tag{4.6}$$

with $K = \mu b^2/(4\pi D^2(1-\nu))$. If an external stress field $\tau(\vec{r})$ is applied, an equation of motion for the nth dislocation in the grain boundary ensues

$$\gamma \dot{\eta}_n + \frac{\delta E}{\delta \eta_n} = sb\tau(\vec{r}), \tag{4.7}$$

where γ is a phenomenological friction coefficient for dislocation glide. The static displacement is then obtained as the solution of

$$\frac{\delta E}{\delta \eta_n} = \sum_m V_{nm}\eta_m = sb\tau(\vec{r}), \tag{4.8}$$

where

$$V_{nm} = \begin{cases} -K\frac{1}{(n-m)^2}, & n \neq m \\ K\sum_{k\neq n}\frac{1}{(n-k)^2}, & n = m. \end{cases} \tag{4.9}$$

If one takes $\tau(\vec{r})$ to be the stress field generated by a single external edge dislocation a having a Burgers vector of modulus b and sign $s_a = \pm 1$, positioned at $\vec{r}_a = (x_a, y_a)$, Eq. (4.8) becomes

$$\sum_m V_{nm}\eta_m = ss_a c(\eta_n - x_a)\frac{(\eta_n - x_a)^2 - (Dn - y_a)^2}{[(\eta_n - x_a)^2 + (Dn - y_a)^2]^2}, \tag{4.10}$$

where $c = \mu b^2/[2\pi(1-\nu)]$. By assuming small deformations $\eta_n \ll x_a$, and expanding to the lowest order in η_n, one obtains the solution

$$\eta_n \approx -x_a \sum_l \lambda_l^{-1}\gamma_n^l \sum_m \gamma_m^l C_m(\vec{r}_a), \tag{4.11}$$

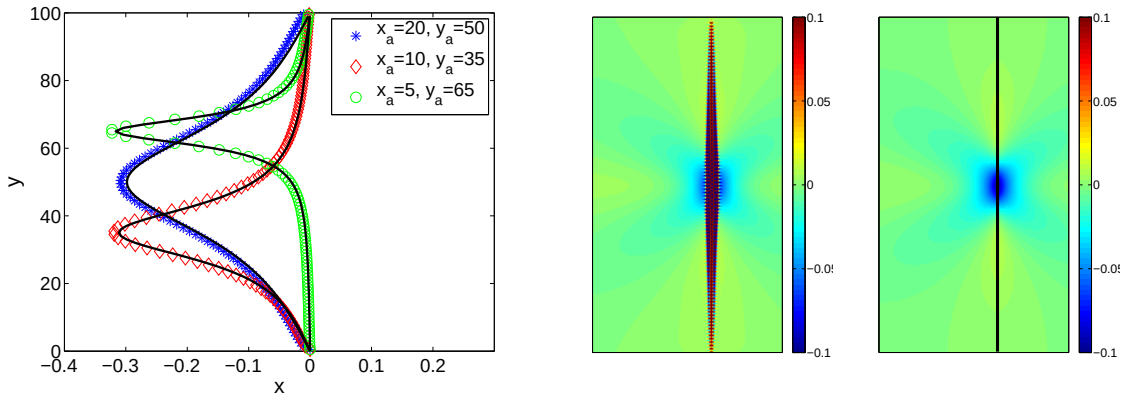

Figure 4.7: Left: Comparison between Eq.(4.12) and the profiles of the deformed grain boundaries obtained from the discrete dislocation dynamics simulations. Middle: The deformation induced stress correction to the stress field of a straight grain boundary, as obtained from discrete dislocation dynamics simulations, by computing the difference between the deformed and undeformed cases. Right: The first order correction term, Eq. (4.15).

where $\lambda_l = 2K\pi l/N$ and $\gamma_n^l = \sqrt{2/N}\sin \pi ln/N$ are the eigenvalues and eigenvectors of the matrix V_{nm}, respectively, and $C_n(\vec{r}_a) = ss_a c[x_a^2 - (Dn - ya)^2]/[x_a^2 + (Dn - y_a)^2]^2$. Then, by considering the limit $L \gg x_a$, the sum over m can be replaced by an integral from $-\infty$ to ∞, which is then calculated by considering the residues around the poles of the function $C_m(\vec{r}_a)$. This yields a displacement

$$\eta_n = -2ss_a x_a \frac{1}{N} \sum_l e^{-\frac{\pi l}{L}|x_a|} \sin \frac{\pi l y_a}{L} \sin \frac{\pi ln}{N}. \tag{4.12}$$

This deformation affects the stress field generated by the grain boundary. The shear stress at (x,y) due to the deformed grain boundary can be written as

$$\sigma(x, y) = \sum_n \sigma_n(x - \eta_n, y - y_n). \tag{4.13}$$

For small deformations η_n, the stress can be expressed by Taylor expanding around $\eta_n = 0$, $\sigma_n(x - \eta_n, y - y_n) \approx \sigma_n(x, y - y_n) + \sigma_n'(x, y - y_n)\eta_n + \mathcal{O}(\eta_n^2)$. Eq. (4.13) can then be rewritten as

$$\sigma(x, y) = \sigma^{(0)}(x, y) + \sigma^{(1)}(x, y) + ... \tag{4.14}$$

where $\sigma^{(0)}(x,y)$ is the stress field generated by a straight grain boundary. The first order correction reads

$$\begin{aligned}\sigma^{(1)}(x,y) &= \pi s_a x_a \frac{\mu b}{1-\nu}\frac{1}{L^2}\sum_l e^{-\frac{\pi l|x_a|}{L}}\sin\frac{\pi l y_a}{L}\times \\ &\quad \times l\left(1-\frac{\pi l|x|}{L}\right)e^{-\frac{\pi l|x|}{L}}\sin\frac{\pi l y}{L}.\end{aligned} \tag{4.15}$$

Comparison with results from discrete dislocation dynamics simulations shows that Eqs. (4.12) and (4.15) give a good estimate of the grain boundary deformation due to the external dislocation and the induced stress correction to the grain boundary stress fields, respectively, see Fig. 4.7. The net effect of the grain boundary deformation is such that the deformation-induced stress correction tends to screen the stress field of the external dislocation. Consequently, such a screening effect could provide one mechanism through which avalanches of dislocation activity would tend to be confined to some extent within individual grains. One should note, however, that the deformation process is not instantaneous. Instead, it is characterized by a relaxation time given by [67]

$$\tau = \frac{2LD\gamma(1-\nu)}{\mu b^2}. \tag{4.16}$$

Thus, for very fast avalanches (which may not cross grain boundaries anyway), the relaxation time can be long compared to the avalanche duration, and the screening effect does not play a role. For longer avalanches, however, the deformation-induced screening might become important.

It is important to remember that real grain boundaries present in polycrystalline materials are typically complicated structures which cannot in general be described as an array of dislocations. However, such a simple toy model may nevertheless give some insight on the general physics of screening of stress fields by extended defects such as low angle grain boundaries.

5 Mobile impurities

In this Section, a single particle interacting with a cloud of mobile impurities is studied, as a toy model of a dislocation interacting with diffusing solute atoms in solid solutions. In systems such as metallic alloys, the dynamic interaction of dislocations and the diffusing solute atoms is known to give rise to intriguing phenomenology, including the Portevin-Le Chatelier effect [68]. Here, within the simple toy model of a single "dislocation" interacting with diffusing impurities in one dimension, it is found that the statistical properties of the dynamics of the particle (or "dislocation") can be described by fluctuations characterized by power law scaling with a cut-off. The results are reported in more detail in article **VI**.

5.1 Introduction

The motion of driven particles, interfaces, membranes etc. in disordered media is an important topic in both condensed matter and statistical physics. The properties of *quenched*, or frozen disorder do not change within the experimentally relevant time scales. Such disorder is typically due to various impurities in the material and can be modelled e.g. by pinning centers that have fixed positions in space. For elevated temperatures, however, these impurities might start diffusing around, thus becoming mobile. A particular example of such a system is given by a dislocation interacting with diffusing solute atoms in metallic alloys. The presence of mobile impurities can have dramatic effects on the dynamics of the system, as evidenced e.g. by the Portevin-Le Chatelier -effect in solid solutions [68], occurring within a certain range of temperatures and applied strain rates. This phenomenon, widely believed to arise due to the dynamic interaction between dislocations and diffusing solute atoms, gives rise to localized plastic deformation visible as macroscopic deformation bands and oscillating stress-strain curves of various kinds [69, 70, 71].

5.2 Particle interacting with diffusing impurities

Here, a simplified model mimicking some features of a single dislocation interacting with a cloud of diffusing solute atoms is studied. The dislocation line is reduced to a single point particle, representing the average position of the dislocation line within its glide plane. As thermal fluctuations acting on the different segments of the dislocation tend to average out on the scale of the entire dislocation line, the projection particle is taken to be at zero temperature. The diffusing impurities, mimicking pure misfit solute atoms, have an attractive interaction with the particle (dislocation), but do not interact with each other. For simplicity, the dynamics of the system is constrained to one dimension, and only parameter values of the problem with which the impurity particles have a vanishingly small probability to escape from the neighbourhood of the particle within the relevant time scales are considered. Thus, the particle moves around due to interaction with a cloud composed of a fixed number N of diffusing impurity particles.

The equations of motion of the system are

$$\begin{aligned} \mu\partial_t x &= \sum_i f(x - x_{s,i}) \\ \partial_t x_{s_i} &= -f(x - x_{s,i}) + \eta_i, \end{aligned} \tag{5.1}$$

where x and $x_{s,i}$ are the positions of the particle and the ith impurity particle, respectively. $f(z)$ is the interaction force between the particle and an impurity particle, μ defines the relative mobilities of the particle and the impurities, and η_i is Gaussian white noise acting on the ith impurity particle, with mean zero and standard deviation $\delta\eta$.

By differentiating the equation of motion of the particle with respect to time, and by linearizing the particle-impurity interaction force such that $\partial_z f(z) \approx -C < 0$, one can write an equation of the form of an Ornstein-Uhlenbeck process for $\partial_t x$,

$$\partial_t^2 x = -\lambda\partial_t x + \xi, \tag{5.2}$$

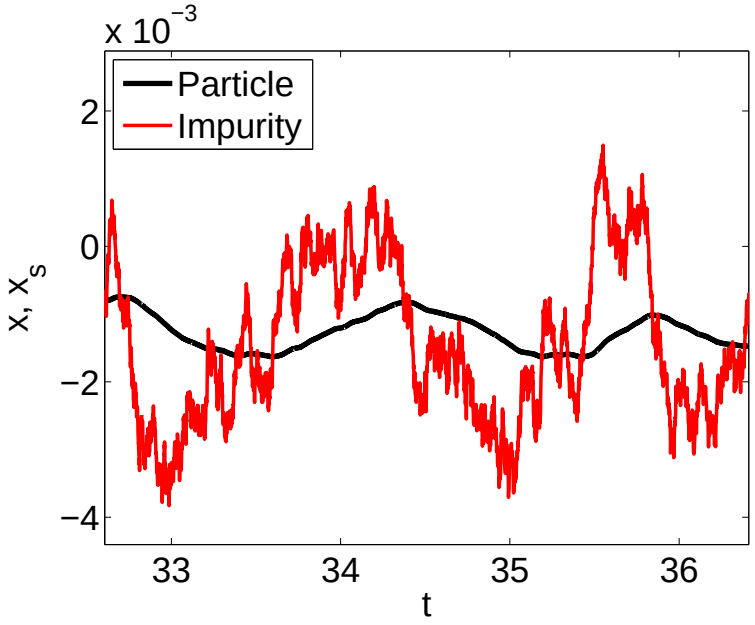

Figure 5.1: Trajectories of the particle and a single impurity. The monotonic excursions correspond to the motion of the particle during time intervals the impurity spends on a given side of the particle. $\mu = A = l = 1.0, \delta\eta = 0.1$.

with $\lambda = C(N+\mu)/\mu$ and $\xi = (C/\mu)\sum_i \eta_i$. The process defined by Eq. (5.2) for $\partial_t x$ has been considered in the literature [72, 73] and its properties are known. In particular, the first passage probability $P(T|v_0)dT$ that the process starting initially at v_0 crosses zero for the first time in $[T, T+dT]$ has an exact expression [73]

$$P(T|v_0) = \sqrt{\frac{2}{\pi D}} \frac{|v_0|\lambda^{3/2} e^{-\lambda T}}{(1-e^{2\lambda T})^{3/2}} \exp\left[-\frac{\lambda v_0^2}{2D(e^{2\lambda T}-1)}\right], \tag{5.3}$$

which vanishes for $v_0 = 0$. To circumvent this problem, a small but non-zero value $v_0 \sim \epsilon$ is considered and Eq. (5.3) is expanded to leading order in ϵ, yielding

$$P(T|\epsilon) \to \epsilon T^{-3/2} f_c(T/T_0), \tag{5.4}$$

where $T_0 = 1/\lambda$ and

$$f_c(x) = \sqrt{\frac{2}{\pi D}} \frac{x^{3/2} e^{-x}}{(1-e^{-2x})^{3/2}}. \tag{5.5}$$

For practical purposes, the first return times T to origin of $\partial_t x$ can thus be taken

to be characterized by a probability distribution scaling as

$$P(T) \sim T^{-\tau_T} f_c\left(\frac{T}{T_0}\right), \tag{5.6}$$

with $\tau_T = 3/2$ and the cut-off scale $T_0 \sim 1/\lambda$. The average shape of an excursion of $\partial_t x$, $\langle \partial_t x(t) \rangle_T$, scales for $t, T - t \ll 1/\lambda$ as $\langle \partial_t x(t) \rangle_T = T^{\gamma_{st}-1} f_{shape}(t/T)$, where $\gamma_{st} = 3/2$. Then, the distribution of lengths $\Delta x = \int_0^T \partial_t x dt$ of the *monotonic excursions* of the particle scales as

$$P(\Delta x) \sim (\Delta x)^{-\tau_{\Delta x}} f_c\left(\frac{\Delta x}{\Delta x_0}\right). \tag{5.7}$$

The exponent value follows from the scaling relation $\tau_{\Delta x} = 1 + (\tau_T - 1)/\gamma_{st}$ [14], yielding $\tau_{\Delta x} = 4/3$. The cut-off scale Δx_0 is due to the combined effect of the cut-off T_0 of the first return time distribution through $\Delta x_0 \sim T_0^{\gamma_{st}}$ and the factors contained in the rescaled noise term, giving rise to

$$\Delta x_0 = \left(\frac{1}{\lambda}\right)^{3/2} \cdot \delta\xi = \sqrt{\frac{\mu}{C}} \frac{\delta\eta}{(1+\mu)^{3/2}}. \tag{5.8}$$

These predictions are verified by numerical simulations, where an interaction force of the form $f(z) = -Az \exp -(1/2)(z/l)^2$ is used for simplicity. The equations of motion (5.1) are integrated with the Euler algorithm. The thermal noise was chosen to be weak enough such that the impurity particles did not escape from the neighbourhood of the particle during the simulation time. An example of the ensuing trajectories for the particle and a single impurity is shown in Fig. 5.1. Probability distributions of the monotonic excursions Δx of the particle are shown in the left panel of Fig. 5.2, displaying the expected scaling with $\tau_{\Delta x} = 4/3$ and the cut-off Δx_0 obeying Eq. (5.8).

The power law forms of the distributions of the monotonic excursions Δx and their durations T indicate that for scales smaller than those corresponding to the cut-offs of the distributions, the particle is performing transient anomalous diffusion. As the early time behaviour of the mean square displacement $\langle x^2 \rangle(t)$ is dominated by

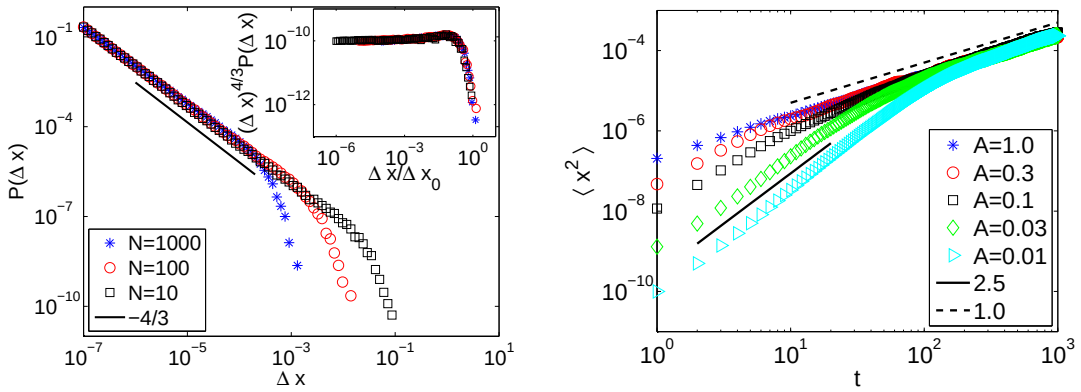

Figure 5.2: Left: The probability distributions of the monotonic excursions of the particle interacting with N impurities. The inset shows a data collapse of the distribution, with Δx_0 computed from Eq. (5.8). Right: The mean squared displacement of the particle interacting with a single impurity, from various interaction strengths A. The early time behaviour follows $\langle x^2 \rangle \sim t^{5/2}$, with a cross-over to normal diffusion for times longer than T_0. $\mu = l = 1.0, \delta\eta = 0.1$.

a single large step Δx, one should consider the effect of such a step conditioned on its duration,

$$\langle x^2 \rangle(t) \sim \int_0^t [\Delta x(T)]^2 P(T) dT = \int_0^t T^{2\gamma_{st}-\tau_T} dT \sim t^{2\gamma_{st}-\tau_T+1}, \tag{5.9}$$

corresponding to $\langle x^2 \rangle(t) \sim t^{5/2}$. For times longer than T_0, a cross-over to normal diffusion with $\langle x^2 \rangle(t) \sim t$ is expected. The right panel of Fig. (5.2) shows the behaviour of $\langle x^2 \rangle(t)$ in numerical simulations, confirming the above result.

5.3 Constant velocity drive

To study the effect of an external drive, a slow constant velocity drive is considered. The equations of motion become

$$\begin{aligned} \mu \partial_t x &= \sum_i f(x - x_{s,i}) + F \\ \partial_t x_{s_i} &= -f(x - x_{s,i}) + \eta_i, \end{aligned} \tag{5.10}$$

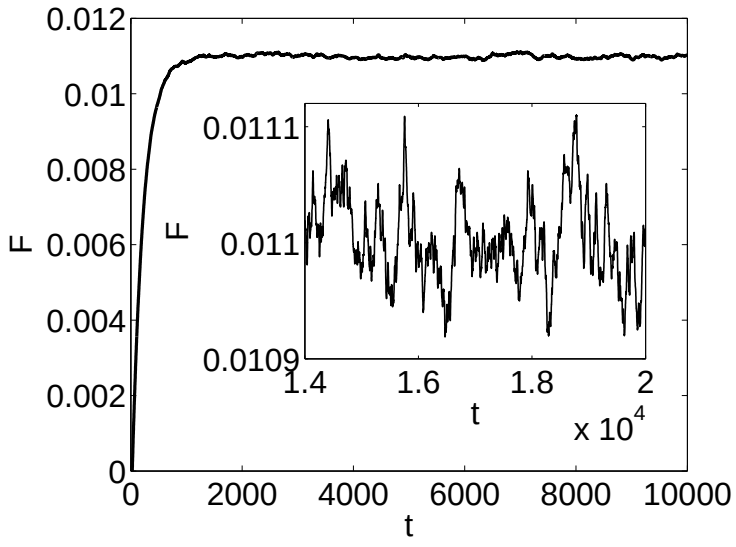

Figure 5.3: The behaviour of the external force as a function of time. The inset shows a magnification of a part of the signal in the steady state. $\mu = l = 1.0, A = 0.01, N = 10, K = 0.1, \delta\eta = 0.1$ and $V = 0.001$.

where $F = K(Vt - x)$, with V the driving velocity and K a spring constant characterizing the response of the driving mechanism. Here, the interesting quantity is the statistics of the external force fluctuations. An example of the behaviour of the external force as a function of time is shown in Fig. 5.3. After an initial transient, the system enters a steady state characterized by fluctuations of the external force. To study such fluctuations, the stochastic process $\partial_t F$ is considered, along similar ideas as above. One can thus write

$$\begin{aligned} \partial_t^2 F &= -K\partial_t^2 x \\ &= -\left[\frac{K}{\mu} + \frac{C}{\mu}(N+\mu)\right]\partial_t F + \frac{KC}{\mu}\sum_i \eta_i \\ &\quad + \frac{KC}{\mu}[V(N+\mu) - F]. \end{aligned} \tag{5.11}$$

In the steady state the last term has a zero mean, due to the balance of the driving velocity and the average retarding force due to a single impurity. By further assuming that its fluctuations $\delta[V(N+\mu) - F] = \delta F$ satisfy $\delta F \ll \sqrt{N}\delta\eta$, Eq. (5.11) can

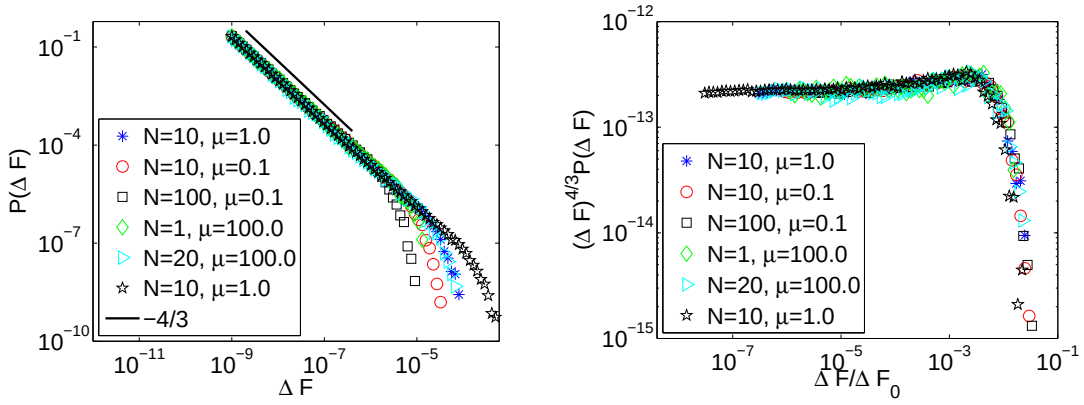

Figure 5.4: Left: The probability distributions of the monotonic changes of the external force ΔF for various parameter values. Right: A data collapse of the same distributions, with F_0 computed from Eq. (5.13)

be approximately written as

$$\partial_t^2 F = -\left[\frac{K}{\mu} + \frac{C}{\mu}(N+\mu)\right]\partial_t F + \frac{KC}{\mu}\sum_i \eta_i, \tag{5.12}$$

which is again of the form of the Ornstein-Uhlenbeck process for $\partial_t F$. Thus, the monotonic changes of the external force $\Delta F = \int_0^T \partial_t F dt$ are expected to be distributed as a power law $P(\Delta F) \sim (\Delta F)^{-\tau_{\Delta F}} f_c(\Delta F/\Delta F_0)$, with $\tau_{\Delta F} = 4/3$ and

$$\Delta F_0 = \frac{KC\sqrt{\mu N}\delta\eta}{[K + C(N+\mu)]^{3/2}}. \tag{5.13}$$

Fig. 5.4 shows the probability distributions $P(\Delta F)$ for various values of the parameters satisfying the condition $\Delta F_0 \ll \sqrt{N}\delta\eta$. The expected power law scaling with $\tau_{\Delta F} = 4/3$ and ΔF_0 obeying equation (5.13) is observed.

The fluctuations considered here have been neglected in classical studies of a dislocation dragging a cloud of solute atoms [74]. Future studies of these issues in systems with a large number of interacting dislocations interacting with diffusing solute atoms would be interesting.

6 Summary

In this thesis various aspects of non-equilibrium systems with avalanche dynamics are studied. The relation between the power spectrum and avalanche scaling originally proposed to account for observations in the context of Barkhausen noise is shown to be applicable much more generally. In article **I**, for the sandpile models of self-organized criticality this is shown to imply that such simple models can exhibit non-trivial scaling of the high frequency power spectrum of the activity time series $V(t)$, contrary to earlier claims. Thus, observations of a power spectrum exponent $\alpha < 2$ in various systems, such as in the context of solar flares [75, 76], cannot be used to exclude SOC as the underlying mechanism.

In article **II**, the same relation between the avalanche statistics and the power spectrum scaling is demonstrated to apply also for the spatially averaged velocity of an advancing fluid front when a viscous fluid displaces air or a less viscous fluid in porous media (imbibition) within a phase field model of the problem. Furthermore, also the collective dislocation activity in a simple two dimensional dislocation dynamics model obeys the same scaling relation (article **III**), which could be checked also in three dimensional simulations [53] and possibly in experiments [13]. This scaling appears thus to be quite generally applicable in systems with avalanche dynamics.

In article **II** it is also found that the velocity fluctuations of the fluid interface exhibit scaling with the average interface velocity that is governed by the geometry of the situation as well as by the conservation law arising from the liquid conservation. This is then contrasted with the velocity fluctuations of interfaces without any conservation law, which are found to obey different scaling. These findings can be checked experimentally in systems such as Hele-Shaw cells.

Several aspects of the rich phenomenology arising from the interaction of large num-

bers of dislocations in plastically deforming crystals are further considered in articles **IV** and **V** within the two-dimensional discrete dislocation dynamics model. In article **IV**, the effects of the threshold value used to identify individual avalanches on the observed correlations between such avalanches are studied. As thresholding of the intermittent signal is typically used also in various experimental situations, the evolution of the waiting time distributions with the imposed threshold could explain some of the observed non-trivial distributions in such experiments. Also the ageing behaviour of the system in repeated loading/unloading cycles is studied, and clear history dependence of the response of the system to the loading stress is observed. These issues should be studied in more detail in the future. In article **V**, the interaction of a single dislocation with an array of dislocations - a toy model of a deformable grain boundary - is studied. The relevance of the grain boundary deformation induced screening on the propagation of avalanches of plastic activity in polycrystalline materials is discussed. An interesting possibility would be to study such phenomena experimentally e.g. in colloidal crystals [77].

Finally in article **VI**, a single particle interacting with a cloud of diffusing impurities is studied, as a toy model of a dislocation interacting with a cloud of solute atoms in solid solutions. Analytical calculations and numerical results show that the dynamics of such a system can be described by fluctuations with statistics given by power law distributions with a cut-off. It would be interesting to study the effect of such fluctuations on larger scales, by considering numerically the dynamics of systems with large numbers of interacting dislocations interacting with diffusing solute atoms.

References

[1] J. P. Sethna, K. A. Dahmen, and C. R. Myers, Nature **410**, 242 (2001).

[2] P. A. Houle and J. P. Sethna, Phys. Rev. E **54**, 278 (1996).

[3] L. I. Salminen, A. I. Tolvanen, and M. J. Alava, Phys. Rev. Lett. **89**, 185593 (2002).

[4] B. Gutenberg and C. F. Richter, *Seismicity of the Earth and Associated Phenomena* (Princeton Univ. Press, Princeton, 1954).

[5] H. Barkhausen, Z. Phys. **20**, 401 (1919).

[6] P. Cizeau, S. Zapperi, G. Durin, and H. E. Stanley, Phys. Rev. Lett. **79**, 4669 (1997).

[7] D.-H. Kim, S.-B. Choe, and S.-C. Shin, Phys. Rev. Lett. **90**, 087203 (2003).

[8] M. J. Alava, M. Dube, and M. Rost, Adv. Phys. **53**, 83 (2004).

[9] D. Geromichalos, F. Mugele, and S. Herminghaus, Phys. Rev. Lett. **89**, 104503 (2002).

[10] J. Soriano, A. Mercier, R. Planet, A. Hernandez-Machado, M. A. Rodrigues, and J. Ortin, Phys. Rev. Lett. **95**, 104501 (2005).

[11] M. Zaiser, Adv. Phys. **55**, 185 (2006).

[12] M.-C. Miguel, A. Vespignani, S. Zapperi, J. Weiss, and J.-R. Grasso, Nature **410**, 667 (2001).

[13] D. M. Dimiduk, C. Woodward, R. LeSar, and M. D. Uchic, Science **312**, 1188 (2006).

[14] S. Lubeck, Int. J. Mod. Phys. B **18**, 3977 (2004).

[15] P. Bak. C. Tang, and K. Wiesenfeld, Phys. Rev. Lett. **59**, 381 (1987).

[16] J. Koivisto, J. Rosti, and M. J. Alava, Phys. Rev. Lett. **99**, 145504 (2007).

[17] F. Omori, J. College Sci. Imper. Univ. Tokyo **7**, 111 (1895).

[18] J. Weiss and D. Marsan, Science **229**, 89 (2003).

[19] T. Richeton, J. Weiss, and F. Louchet, Acta Mater. **53**, 4463 (2005).

[20] L. Laurson, M. J. Alava, and S. Zapperi, J. Stat. Mech.: Theo. Exp., L11001 (2005).

[21] L. Laurson and M. J. Alava, Phys. Rev. E **74**, 066106 (2006).

[22] M. Rost, L. Laurson, M. Dube, and M. J. Alava, Phys. Rev. Lett. **98**, 054502 (2007).

[23] M. C. Kuntz and J. P. Sethna, Phys. Rev. B **62**, 11699 (2000).

[24] A. P. Mehta, A. C. Mills, K. A. Dahmen, and J. P. Sethna, Phys. Rev. E **65**, 046139 (2002).

[25] S. Zapperi, C. Castellano, F. Colaiori, and G. Durin, Nature Physics **1**, 46 (2005).

[26] H. J. Jensen, *Self-Organized Criticality: Emergent Complex Behaviour in Physical and Bilogical Sytems* (Cambridge University Press, 1998).

[27] S. S. Manna, J. Phys. A: Math. Gen. **24**, L363 (1991).

[28] R. Dickman, M. Alava, M. A. Muõz, J. Peltola, A. Vespignani, and S. Zapperi, Phys. Rev. E **64**, 056104 (2001).

[29] M. Alava and K. B. Lauritsen, Europhys. Lett. **53**, 569 (2001).

[30] M. Alava, J. Phys.: Condens. Matter **14**, 2353 (2002).

[31] M. J. Alava, L. Laurson, A. Vespignani, and S. Zapperi, Phys. Rev. E **77**, 048101 (2008).

[32] C. Tebaldi, M. De Menech, and A. L. Stella, Phys. Rev. Lett. **83**, 11699 (1999).

[33] H. J. Jensen, K. Christensen, and H. C. Fogedby, Phys. Rev. B **40**, R7425 (1989).

[34] J. Kertesz and L. B. Kiss, J. Phys. A: Math. Gen. **23**, L433 (1990).

[35] T. Hwa and M. Kardar, Phys. Rev. A **45**, 7002 (1992).

[36] S. Maslov, C. Tang, and Y. C. Zhang, Phys. Rev. Lett. **83**, 2449 (1999).

[37] A. A. Ali, Phys. Rev. E **52**, R4595 (1995).

[38] J. Davidsen and M. Paczuski, Phys. Rev. E **66**, 050101 (2002).

[39] D. Zhou, L. Jia, J. Kamath, and A. R. Kovscek, J. Pet. Sci. Eng. **33**, 61 (2002).

[40] J. Rosinski, Am. Ink Maker **71**, 40 (1993).

[41] E. W. Washburn, Phys. Rev. **17**, 273 (1921).

[42] M. Sahimi, Rev. Mod. Phys. **65**, 1393 (1993).

[43] M. Dube, M. Rost, K. R. Elder, M. Alava, S. Majaniemi, and T. Ala-Nissilä, Phys. Rev. Lett. **83**, 1628 (1999).

[44] E. Paune and J. Casademunt, Phys. Rev. Lett. **90**, 144504 (2003).

[45] J. Weiss, J.-R. Grasso, M.-C. Miguel, A. Vespignani, and S. Zapperi, Mater. Sci. Eng. A **309-310**, 360 (2001).

[46] J. Weiss and D. Marsan, Science **229**, 89 (2003).

[47] M. Zaiser, F. M. Grassett, V. Koutsos, and E. C. Aifantis, Phys. Rev. Lett. **93**, 195507 (2004).

[48] J. Weiss and J.-R. Grasso, J. Phys. Chem. B **101**, 6113 (1997).

[49] C. A. Schuh and T. G. Nieh, Acta Mater. **51**, 87 (2003).

[50] B. Miller, C. O'Hern, and R. P. Behringer, Phys. Rev. Lett. **77**, 3110 (1996).

[51] E. Pratt and M. Dennin, Phys. Rev. E **67**, 051402 (2003).

[52] M.-C. Miguel, A. Vespignani, S. Zapperi, J. Weiss, and J.-R. Grasso, Mater. Sci. Eng. A **309-310**, 324 (2001).

[53] F. Csikor, C. Motz, D. Weygand, M. Zaiser and S. Zapperi, Science **318**, 251 (2007).

[54] M. Koslowski, R. LeSar, and R. Thomson, Phys. Rev. Lett. **93**, 125502 (2004).

[55] V.S. Deshpande, A. Needleman, and E. Van der Giessen, Acta Mater. **50**, 831 (2002).

[56] S. J. Zhou, D. L. Preston, P. S. Lomdahl, and D. M. Beazley, Science **279**, 1525 (1998).

[57] Y. Huang, S. Qu, K. C. Hwang, M. Li, H. Gao, Int. J. Plasticity **20**, 753 (2004).

[58] G. Ananthakrishna and M. S. Bharathi, Phys. Rev. E **70**, 026111 (2004).

[59] A. Arsenlis, B. D. Wirth, and M. Rhee, Phil. Mag. **84**, 3617 (2004).

[60] J. Rabier, F. Sandiumenge, J. Plain, A. Proult, and I. Stretton, Phil. Mag. Lett. **82**, 419 (2002).

[61] A. H. Cottrell and V. Aytekin, Nature **160**, 328 (1947).

[62] J. Rosti *et al.*, in preparation.

[63] B. Bako, I. Groma, G. Györgyi, and G. T. Zimanyi, Phys. Rev. Lett. **98**, 075701 (2007).

[64] V. Taupin, T. Richeton, J. Chevy, C. Fressengeas, J. Weiss, F. Louchet, and M.-C. Miguel, Acta Mater. **56**, 1555 (2008).

[65] T. Richeton, J. Weiss, and F. Louchet, Nature Materials **4**, 465 (2005).

[66] F. Louchet, J. Weiss, and T. Richeton, Phys. Rev. Lett. **97**, 075504 (2006).

[67] R. Bruinsma, B. I. Halperin, and A. Zippelius, Phys. Rev. B **25**, 579 (1982).

[68] A. Portevin and F. Le Chatelier, C. R. Acad. Sci. Paris **176**, 507 (1923).

[69] G. Ananthakrishna, S. J. Noronha, C. Fressengeas, and L. P. Kubin, Phys. Rev. E **60**, 5455 (1999).

[70] M. A. Lebyodkin, Y. Brechet, Y. Estrin, and L. P. Kubin, Phys. Rev. Lett. **74**, 4758 (1995).

[71] P. Hähner, A. Ziegenbein, E. Rizzi, and H. Neuhäuser, Phys. Rev. B **65**, 134109 (2002).

[72] F. Colaiori, A. Baldassarri, and C. Castellano, Phys. Rev. E **69**, 041105 (2004).

[73] S. N. Majumdar, A. J. Bray, and G. C. M. A. Ehrhardt, Phys. Rev. E **64**, 015101(R) (2001).

[74] J. P. Hirth and J. Lothe, *Theory of Dislocations* (John Wiley & Sons 1982).

[75] E. T. Lu and R. J. Hamilton, Astrophys. J. **380**, L89 (1991).

[76] M. Baiesi, M. Paczuski, and A. L. Stella, Phys. Rev. Lett. **96**, 051103 (2006).

[77] P. Lipowsky, M. J. Bovick, J. H. Meinke, D. R. Nelson and A. R. Bausch, Nature Materials **4**, 407 (2005).

ISBN 978-951-22-9536-4
ISBN 978-951-22-9537-1 (PDF)
ISSN 1795-2239
ISSN 1795-4584 (PDF)